



REVIEW

Efficient Application to Remove Arsenic and Antimony from the Water Environment Using Renewable Carbon-Based Materials: A Review

Tongtong Wang^{1,#}, Zhenhui Pan^{2,#}, Di Zhang², Hui Shi^{1,2,*}, Murat Yılmaz³, Amit Kumar⁴, Gaurav Sharma⁴ and Tao Liu^{2,*}

¹Institute for Interdisciplinary and Innovate Research, Xi'an University of Architecture and Technology, Xi'an, 710055, China

²School of Environmental and Municipal Engineering, Xi'an University of Architecture and Technology, Xi'an, 710055, China

³Department of Chemistry and Chemical Processing Technologies, Bahçe Vocational School, Osmaniye Korkut Ata University, Osmaniye, 80000, Türkiye

⁴International Research Centre of Nanotechnology for Himalayan Sustainability (IRC NHS), Shoolini University, Solan, 173229, India

*Corresponding Authors: Hui Shi. Email: shihui@xauat.edu.cn; Tao Liu. Email: liutao1995@xauat.edu.cn

#These authors contributed equally to this work

Received: 21 November 2024; Accepted: 05 February 2025; Published: 23 June 2025

ABSTRACT: With the rapid development of industry, the environmental problems caused by heavy metal arsenic and antimony are becoming increasingly serious. Therefore, it is urgent to solve the problem of arsenic and antimony pollution in the water environment. Renewable carbon-based materials, as a kind of adsorbent widely used in wastewater treatment, have been the focus of scholars' research for many years. In this review, the preparation methods, characteristics, and applications of renewable carbon-based materials (biochar, activated carbon, carbon nanotubes, and graphene) for the removal of arsenic and antimony are described in detail. Based on adsorption kinetics, isothermal adsorption, temperature, pH, and coexisting ions, we discuss the process of adsorption of arsenic and antimony by renewable carbon-based materials, explore the mechanism of adsorption of anions in water by renewable carbon-based materials, and comparatively analyze the differences in adsorption performance of arsenic and antimony by different renewable carbon-based materials. Compared with biochar, activated carbon, carbon nanotube, and graphene renewable materials loaded with iron-manganese oxides have better removal effects on arsenic and antimony wastewater. Extensive research data shows that biochar, as a renewable material, is recommended, followed by activated carbon. Both are recommended because of their excellent adsorption properties and low production costs. Finally, the prospects and challenges of the application of renewable carbon-based materials in wastewater treatment are discussed, and the directions and development trends of future research are pointed out, which provide references and insights for further promoting the application of renewable carbon-based materials in wastewater treatment.

KEYWORDS: Renewable carbon-based materials; arsenic; antimony; adsorption mechanisms; wastewater treatment

1 Introduction

With the rapid development of heavy industry (coal mining, metal smelting) and fine chemical industry, a large amount of wastewater containing arsenic (As) and antimony (Sb) enters the water body, posing a substantial risk to the human health and ecological environment. Unlike other heavy metals, As and Sb, as toxic metals, mostly exist in the form of oxidized negative ionic state in the water body; thus, there are certain peculiarities in the purification and treatment process. In natural water, arsenic predominantly exists as arsenate (As(V)) and arsenite (As(III)), with arsenate exhibiting greater toxicity than arsenite [1,2]. As



enters the human body, it will cause a variety of complications in the human organ system (skin, nerves, cardiovascular, kidney, reproductive system), such as long-term intake of inorganic arsenic in drinking water ($0.05 \text{ mg}\cdot\text{L}^{-1}$ or more), which can cause a variety of skin diseases (hyperpigmentation and hyperkeratosis) and cancers (skin, lungs, kidneys, bladder), which collectively referred to as arsenic poisoning [3]. Therefore, in 1993, the World Health Organization revised the recommended maximum contaminant limit (MCL) guidelines for As in drinking water from 0.05 to $0.01 \text{ mg}\cdot\text{L}^{-1}$ [4]. Sb exists in natural waters, mainly in the Sb(III) and Sb(V) valence states, where Sb(III) is ten times more toxic compared to Sb(V) [5,6]. Sb causes damage to the liver, lungs, and cardiovascular system when humans are exposed to Sb-contaminated water, with acute and chronic toxicity of Sb(V) to humans mainly in the form of pneumoconiosis, respiratory irritation, and gastrointestinal symptoms [7,8]. In China, super-large and large- and medium-sized antimony deposits are concentrated in the provinces of Guangxi (34.4%), Hunan (21.2%), Yunnan (12.2%), and Guizhou (10.2%), with antimony concentrations in surface water around the mines as high as $52.7\text{--}163 \text{ }\mu\text{g}\cdot\text{L}^{-1}$, which is far more than the maximum permissible antimony content in China's drinking water ($5 \text{ }\mu\text{g}\cdot\text{L}^{-1}$), and is seriously jeopardizing the normal life of the surrounding residents [9,10].

To deal with the increasingly serious problem of arsenic and antimony wastewater treatment, various treatment technologies have been widely used in recent decades, including adsorption, membrane, microbial, chemical precipitation, electrochemical, and photocatalytic methods [11–16]. Among these methods, both membrane and chemical precipitation technologies are more mature and practical. However, the sludge produced by the chemical precipitation method is bulky and needs to be settled and separated for reprocessing, which increases the additional cost of the treatment process [12]. The membrane method is more costly to separate and also faces the problem of membrane contamination [11]. Although the microbial method is non-polluting, microorganisms are sensitive to environmental conditions and require specialized operation and management [13]. The photocatalytic method is more popular due to the advantages of utilizing green energy, solar energy, and the absence of secondary harmful by-products, but its treatment efficiency is low [15]. Electrochemistry has the advantage of high treatment efficiency, but the consumption of electric energy is high, and problems such as electrode passivation need to be considered [16]. Compared with the above several treatment methods, the adsorption method is the most researched method in recent years, which offers the benefits of less operational expenses, high removal rate, easy operation, and the adsorbed As and Sb can be recovered by desorption method [13,14]. Extensive adsorption experiments revealed that arsenic (As) and antimony (Sb) interact with various solid-phase adsorbents, including ferromanganese slag [17], montmorillonite [18], magnetic nanomaterials [19], alum sludge [20], layered double hydroxides [19], and renewable carbon-based materials [21,22]. Among them, renewable carbon-based materials, which have the advantages of wide sources [23], large specific surface area [24], reusability [25], and environmental friendliness [26], have received more and more attention from human beings in recent years. Fig. 1 demonstrates the advantages of renewable carbon-based materials for removing As and Sb from water.

There have been many studies using renewable carbon-based materials as adsorbents in reported articles (Fig. 2), which show that renewable carbon-based materials are increasingly emphasized in the field of As and Sb removal. Therefore, it is important to review the latest research progress on the adsorption of As and Sb by renewable materials. In this review, we summarized the synthesis methods of different renewable carbon materials and described their physical and chemical properties in detail. The adsorption characteristics of these materials for the heavy metals As and Sb are discussed extensively, and the most important influencing factors are clarified. This review provides new insights into the adsorption mechanisms of renewable carbon-based adsorbents for As and Sb, and the differences in adsorption capacity and factors affecting the adsorption process are compared and analyzed. Finally, the challenges facing these renewable materials

and potential solutions are prospected, providing a guide for future research and applications of renewable carbon-based adsorbents.

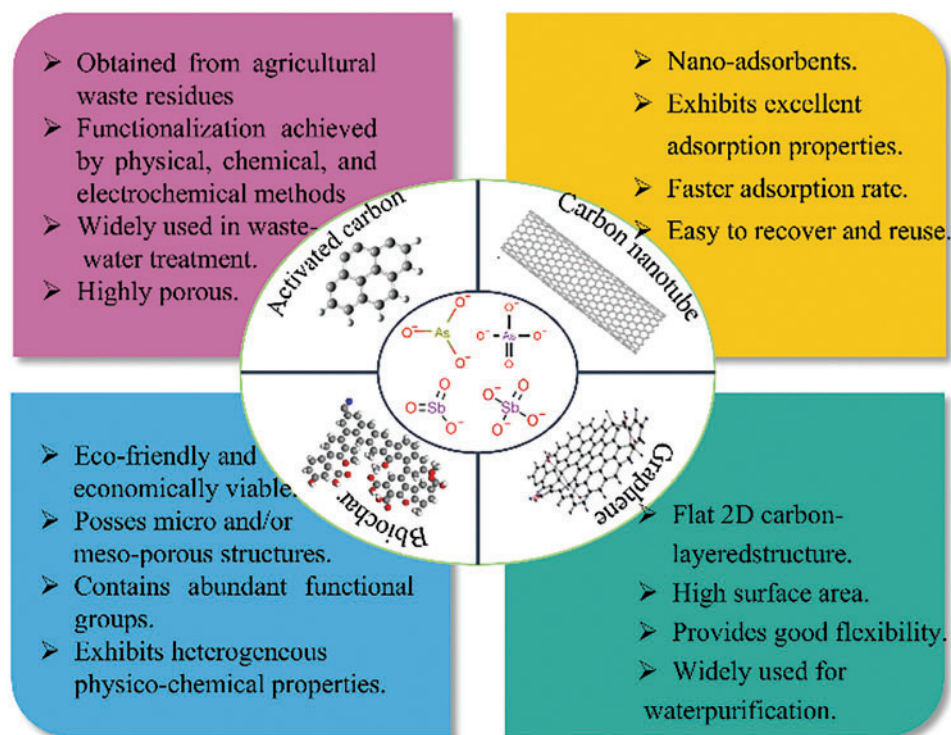


Figure 1: Renewable carbon-based materials for adsorption of As and Sb in water

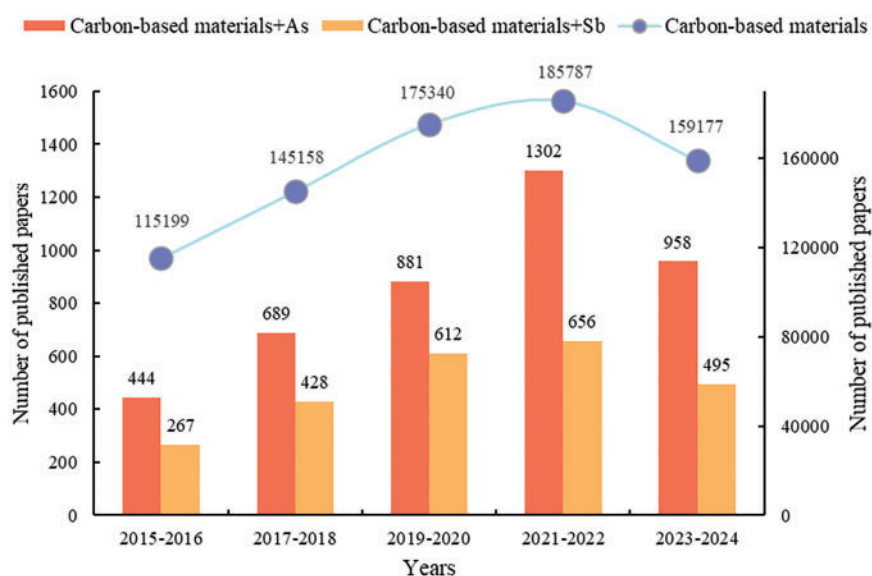
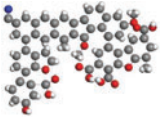
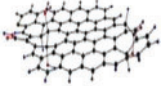
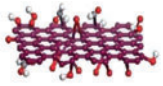




Figure 2: Statistics on the number of publications on “Heavy metals arsenic and antimony” from renewable carbon-based materials (retrieved on 13 November 2024). The number of publications in the Web of Science database is based on the following keywords: “carbon-based materials”, “carbon-based materials and As”, and “carbon-based materials and Sb”

2 Renewable Carbon-Based Materials and Preparation Methods

Through research in recent decades, many types of renewable carbon-based materials have been continuously found to be modified and widely used in heavy metal removal [24]. Numerous experiments have shown that renewable carbon-based materials such as biochar, graphene, carbon nanotubes, and activated carbon can effectively eliminate As and Sb from water and play an important role in wastewater treatment (Table 1).

Table 1: Definition and structure of renewable carbon-based materials

Materials	Definition	Structure	Preparation of raw materials	Ref.
Biochar	A carbonaceous material generated from the burning of organic feedstocks in oxygen-restricted environments at elevated temperatures.		Biomass (cellulose, hemicellulose, and lignin)	[26,27]
Graphene	A monolayer planar sheet of sp^2 hybridized carbon atoms organized in a honeycomb lattice configuration.		Renewable graphite or biomass	[28,29]
Graphene oxide	An oxidized variant of graphene featuring a monatomic carbon layer structure altered on both sides with oxygen-containing functional groups.		Renewable graphite or biomass	[30,31]
Carbon nanotube	Coaxial tubes consist of several to dozens of layers of carbon atoms organized in a hexagonal configuration.		Biomass, renewable carbide, and carbon	[32]
Activated carbon	Carbon materials are prepared from carbonaceous raw materials including coal, wood, and petroleum coke through pyrolysis and activation processing.		Biomass, coal, and petroleum coke, etc.	[33–35]

2.1 Biochar

Biochar is mainly composed of aromatic hydrocarbons, monomeric carbon, or carbon with a graphitic structure, containing more than 60% carbon, as well as H, O, N, S, and small amounts of trace elements [27]. Biochar is prepared from many feedstock sources, including wood, municipal solid waste, crop waste, and organic sludge. Biochar has the advantages of rich carbon content, high ion-exchange capacity, large surface area, and stable structure [26], and these basic properties give it an excellent adsorption capacity, which has been widely emphasized in heavy metal removal from wastewater [27].

The methods of preparing biochar include hydrothermal carbonization, gasification, and pyrolysis, of which the most commonly used method is pyrolytic carbonization, while the charcoal obtained from

gasification and hydrothermal carbonization generally does not meet the definition of biochar [36,37]. Pyrolytic carbonization is the process of thermally decomposing biomass into solids (biochar), gases, and condensed liquids (bio-oil) at high temperatures of 300°C–1000°C in an oxygen-free environment [38]. Pyrolysis is generally categorized into two types, slow pyrolysis and fast pyrolysis, depending on the pressure, temperature, residence time, and rate of warming [39]. Slow pyrolysis is the slow heating (minutes to hours) of material to lower temperatures (350°C–450°C) in the presence of long gas residence times (usually minutes to hours) and large particle sizes (>1 mm), which can result in products with up to 60% biochar by mass [40,41]. In contrast to slow pyrolysis, fast pyrolysis involves adding the feedstock to the reactor after reaching the desired temperature (350°C–450°C) and the residence time is usually a few seconds [41]. Hence, the feedstock needs to be ground into small particles and dried. The product is mainly bio-oil (40%–70%), with a lower yield of biochar (10%–25%) [42,43]. Kim et al. [44] utilized four woody biomasses (oak, eucalyptus, pitch pine, and Japanese cedar) to prepare biochar by fast pyrolysis methods with yields of only 11%–14%. To produce efficient and cost-effective biochar, many researchers also have utilized the preparation furnace to prepare biochar (Fig. 3) [45]. Biochar preparation furnaces are cleaner, with lower emissions of carbon monoxide, hydrocarbons, fine particles, and greenhouse gases (carbon dioxide and methane) [43,45]. Gasification is a thermochemical process that transforms the combustible fraction of biomass fuels into flammable gases (hydrogen, carbon monoxide, and methane) under certain high-temperature conditions (usually higher than 700°C) utilizing oxygen or oxygen-rich substances in the air as a gasifying agent [46]. Because the target product of this method is dominated by combustible gas, its biochar yield is lower than pyrolysis. Hydrothermal carbonization is the process of using water as a reaction medium to convert raw materials into carbon materials, mainly biochar, under certain temperatures (130°C–250°C) and pressure conditions [47]. Hydrothermal carbonization is characterized by energy savings in drying raw material moisture, high conversion rates, and lower reaction temperatures [48].

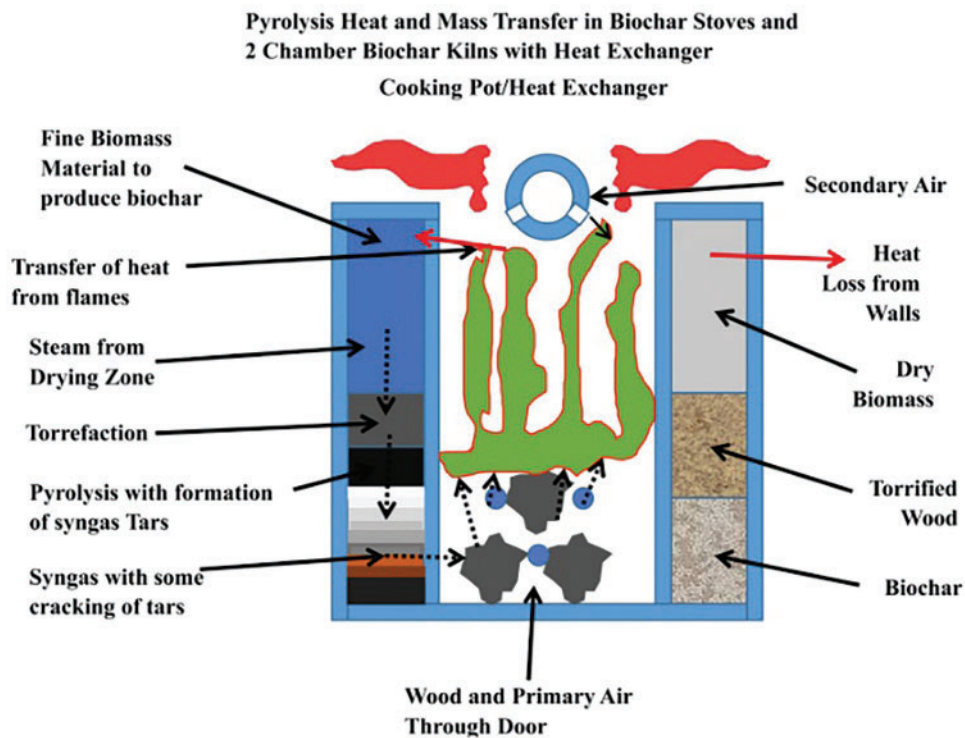


Figure 3: Model of biochar production stoves [45]. Copyright © 2019, Elsevier Ltd.

2.2 Graphene and Oxidation State

In 2004, Novoselov et al. [49] obtained for the first time a stable single-layer two-dimensional crystalline graphite film, graphene, from a graphite sheet using a special adhesive tape (Fig. 4). It exists in the form of carbon flakes with a sp^2 hybridized structure, with unique electron and thermal mobility, excellent corrosion resistance, high mechanical strength, high specific surface area, and tunable surface chemical properties, which have attracted much attention in the field of water treatment [49,50]. Graphene oxide, as the oxidized state of graphene, is abundant in several oxygen-containing functional groups, including -OH, -COOH, etc., and has excellent dispersibility [51].

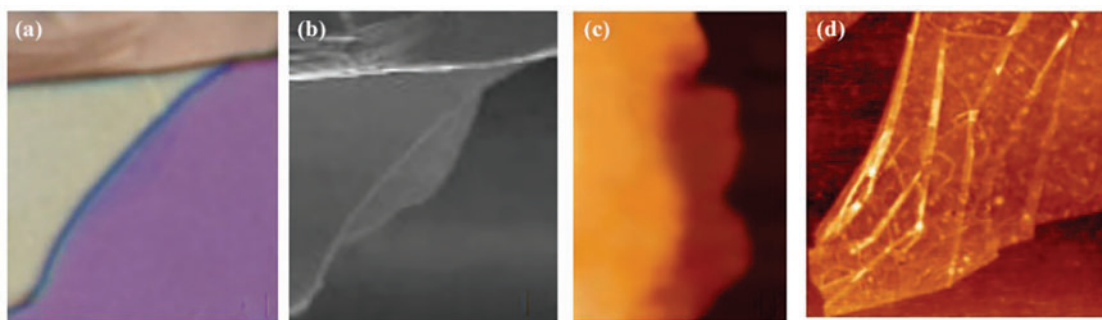


Figure 4: (a) Optical microscopy image of graphene, (b) Scanning electron microscopy image of graphene, (c and d) AFM images of single-layer graphene [49]. Copyright © 2004, American Association for the Advancement of Science

The preparation methods of graphene mainly include mechanical exfoliation and chemical vapor deposition. The mechanical exfoliation method refers to the relative motion and friction between an item and graphene to produce graphene thin layer material. Novoselov et al. [49] initially utilized this method to obtain graphene by exfoliating layers of natural graphite. However, this method has some drawbacks: graphene thickness is not uniform, the yield is very low, and it can not be applied to industrial production on a large scale [49]. Huang et al. [52] invented a simple and effective green mechanical exfoliation method, the soft sphere-microsphere rolling process (Fig. 5). It can realize the large-scale production of graphene with an average layer number of 3.8 ± 1.9 without introducing functional groups or being contaminated [52]. The chemical vapor deposition method refers to the planar substrate (such as metal film, metal single crystal, etc.) placed in a high-temperature decomposable precursor (methane, ethylene, etc.) and then depositing carbon atoms on the surface of the substrate by high-temperature annealing to form graphene [53]. Finally, the metal substrate is removed by chemical etching to obtain individual graphene. Conventional chemical vapor deposition has the disadvantage of slow graphene growth. Ding et al. [54] made it possible for graphene to be synthesized on a molten Ga surface within minutes by using liquid gallium (Ga) as a catalyst. The use of liquid catalysts provides a new way to synthesize graphene efficiently. The synthesis of graphene oxide encompasses both “bottom-up” procedures (such as chemical vapor deposition and epitaxial growth of silicon carbide) and “top-down” techniques [55]. Among them, the extraction of graphene oxide from graphite using the top-down-Hummer method is preferred, which uses sulfuric acid, sodium nitrate, and potassium manganate as oxidizing agents [55]. This method uses sodium nitrate, sulfuric acid, and potassium permanganate as oxidizing agents.

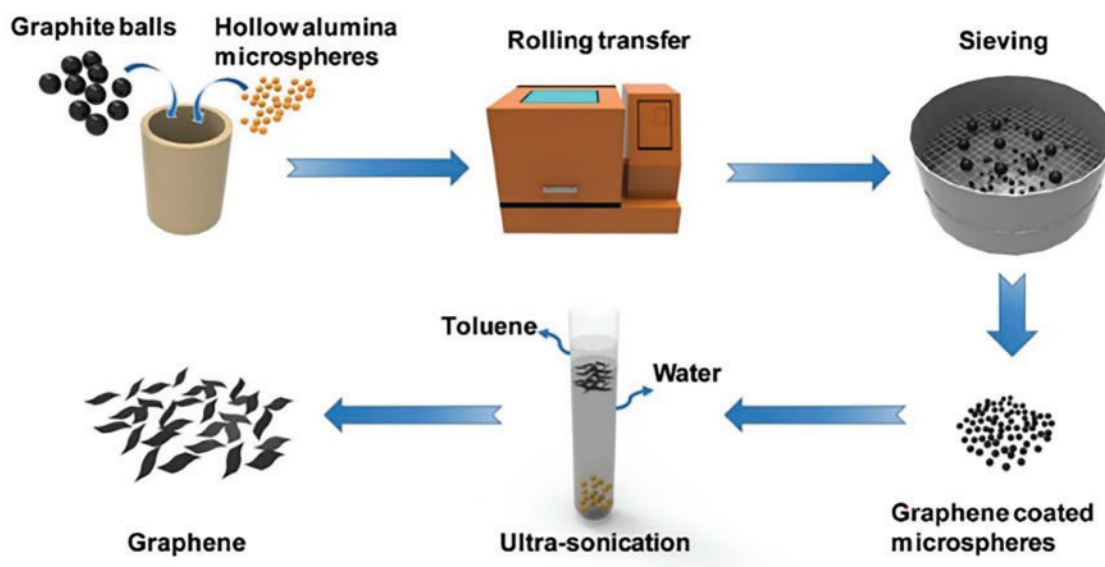


Figure 5: Schematic diagram of graphene soft ball-microsphere rolling transfer process [52]. Copyright © 2019, Elsevier Ltd.

2.3 Carbon Nanotubes

Carbon nanotubes were first discovered in 1991 by the Japanese electron microscopist Iijima during the preparation of C_{60} by the electric arc method [56]. Carbon nanotubes typically consist of one or several layers, classified as single-walled carbon nanotubes (SWCNTs) and multi-walled carbon nanotubes (MWCNTs). SWCNTs have diameters between zero and a few nanometers and lengths of up to a few tens of micrometers, while MWCNTs have diameters between a few nanometers and a few tens of nanometers but lengths of up to a few millimeters [57]. Carbon nanotubes have been popularized as a novel renewable carbon-based adsorbent for wastewater treatment due to their unique structural and excellent electrical, mechanical, and chemical properties (including high specific surface area) [58].

Carbon nanotubes are primarily synthesized using the chemical vapor deposition method, laser ablation method, and arc discharge method. The arc discharge method is to put the graphite electrode in the reaction container filled with inert gas, through the two poles between the excitation of the arc to produce a high temperature of about 4000°C , graphite evaporation to produce single-walled or multi-walled carbon nanotubes [32]. By optimizing the current density and pressure conditions during the arc generation process, Cadek et al. [59] achieved a high yield of carbon nanotubes up to $24 \text{ mg}\cdot\text{min}^{-1}$ with a purity of 48% at a current density of $195 \text{ A}\cdot\text{cm}^{-2}$ and a pressure of 500 Torr. Laser ablation is the process whereby a graphite target containing a metal catalyst is irradiated by laser light and turned into gaseous carbon, which grows into carbon nanotubes under the action of a catalyst as it is carried by a gas stream from the high-temperature region to the low-temperature region [59]. Similar to the arc discharge method, laser ablation also utilizes high-temperature conditions, and the optimal background gas and catalyst mixtures for both methods are very similar. Sarangdevot suggests that the synthesis mechanisms for laser ablation and arc methods may be the same [60]. Thess et al. [61] produced high-quality single-walled carbon nanotubes with greater than 70% content and diameters around 1.38 nm by nickel-cobalt metal catalyzed at 1200°C using the laser ablation method. Chemical vapor deposition (CVD) refers to the thermal degradation of carbonaceous gases (such as carbon monoxide, ethylene, ethane, and ethanol) into atomic constituents, facilitating the interaction of carbon with metal catalysts to synthesize carbon nanotubes (Fig. 6) [62]. Cassell et al. [63] accomplished

the synthesis of substantial amounts of high-quality single-walled carbon nanotubes for the first time by optimizing the catalyst material. The optimized catalyst consisted of Fe/Mo bimetallic substances in a novel silica-alumina multi-component material, which enabled the synthesis of kilogram-scale carbon nanotubes.

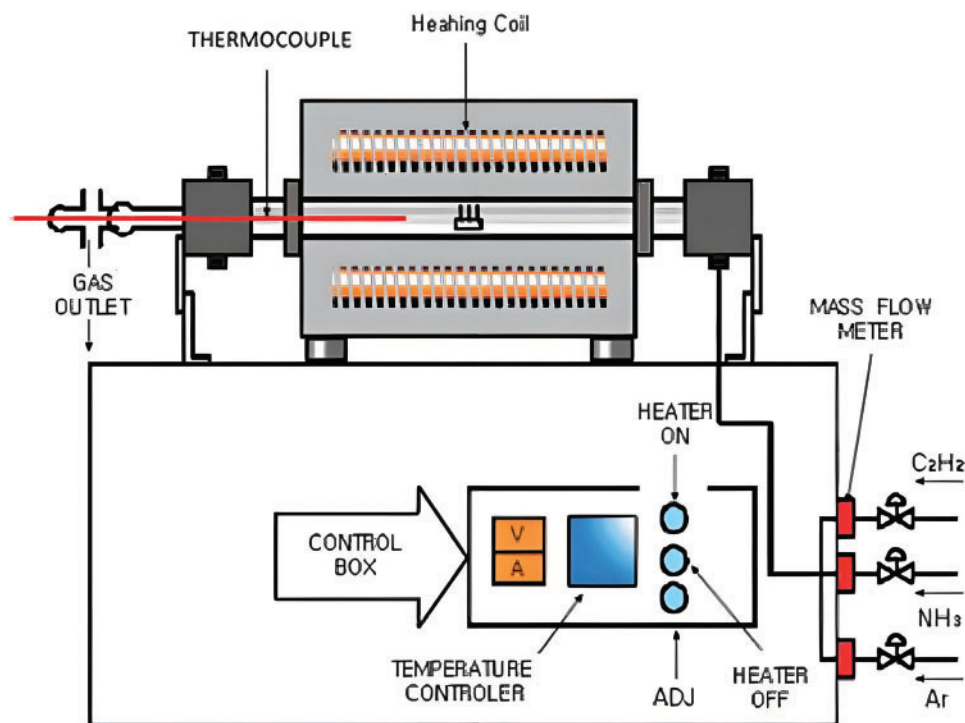


Figure 6: Schematic diagram of chemical vapor deposition apparatus [62]. Copyright Eindhoven University of Technology

2.4 Activated Carbon

Activated carbon is one of the most common adsorbents with a large specific surface porous structure, which is mainly amorphous carbon with small amounts of H, O, N, S, and ash. The micropores of activated carbon are not only rich in number, but also have developed pore structure [64]. The volume of micropores often reaches $0.2\text{--}0.6\text{ cm}^3\cdot\text{g}^{-1}$, which is nearly of the same order of magnitude as the size of the pollutants, so that the pollutants are adsorbed by the superimposed adsorption force of the surrounding pore wall [34]. Additionally, the presence of a large number of oxygen-containing functional groups (carboxyl groups, carbonyl groups, phenols, lactones, and quinones) on the surface of activated carbon improves its adsorption properties [35,65].

Activated carbon preparation mostly occurs through two methods, physical and chemical. The physical method is divided into two steps. Firstly, carbonaceous organic materials will be carbonized at high temperatures, and most of the non-carbon elements will escape in the form of gas to generate carbon-rich pyrolysis products [35]. Secondly, N_2 , CO_2 , or water vapor is used at high temperatures of 800°C – 1000°C for activation, removing the organic matter that cannot be decomposed during carbonization and may erode the surface, forming a developed microporous structure [64,65]. Zhou et al. [66] used a physical method to obtain activated carbon and characterized the pore richness and stability of the activated carbon produced at 800°C activation conditions (Fig. 7). The physical method is a green synthesis method with a relatively simple process flow and produces an exhaust gas dominated by CO_2 and water vapor, which is less polluting

to the environment. However, the activated carbon prepared by this process has a long activation time, low adsorption capacity, and high energy consumption [67]. The chemical method involves soaking and mixing raw materials with activation reagents (H_3PO_4 , ZnCl_2 , etc.) Then heating and activating them in the temperature range of 400°C – 900°C to produce activated carbon [68,69]. Chemical methods require lower activation temperatures, faster processing times, and higher yields than physical methods. Since carbonization and activation co-occur in the chemical preparation, chemical activation can be performed in a single furnace to reduce equipment costs [69]. Hayashi et al. [70] prepared activated carbons with a larger surface area from lignin as raw material using both ZnCl_2 and H_3PO_4 activators at 600°C carbonization temperature. There are also physicochemical activation methods, a combination of physical and chemical activation, whereby the charcoal is first chemically treated and subsequently activated by physical methods (water vapor or CO_2) [70]. The technology has been developed by the Institute of Forest Chemical Industry of the Chinese Academy of Forestry, and a production line with an annual output of 8000 tons has been built in Fujian Yuanli Active Carbon Co., Ltd. [68].

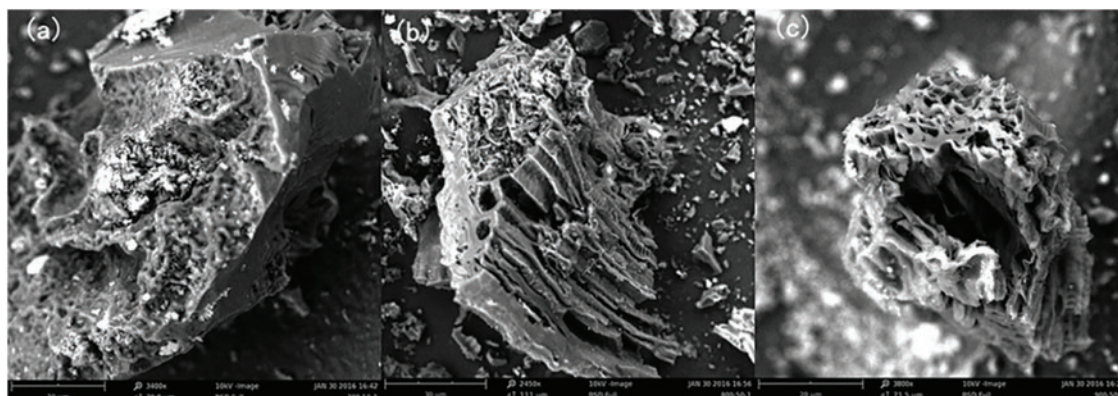


Figure 7: Scanning Electron Microscope (SEM) images of activated carbon at different activation temperatures (a: 700°C , b: 800°C , and c: 900°C) [66]. Copyright © 2018, Taylor & Francis Inc.

3 Removal of As and Sb by Renewable Carbon-Based Materials

3.1 Adsorption Process and Common Environmental Factors

3.1.1 Adsorption Kinetics

By studying the adsorption kinetics of As and Sb on renewable carbon-based materials, the rate, mechanism, and influencing factors of the adsorption process can be understood, which can be used to optimize the performance of renewable carbon-based materials and the design of adsorption systems. The adsorption kinetic model mainly reflects the increase in adsorption capacity with the increase of reaction time until equilibrium is reached. To determine the reaction order and adsorption process, some common adsorption kinetic models are described below:

(1) Pseudo-first-order model: The model is used to describe the monolayer adsorption mainly through boundary diffusion [71].

$$Q_t = Q_e \left(1 - \exp \left(-\frac{k_1}{2.303} t \right) \right) \quad (1)$$

where Q_t is the adsorption amount at time t ($\text{mg}\cdot\text{g}^{-1}$, same below), and k_1 is the pseudo-first-order adsorption rate constant (min^{-1}).

(2) Pseudo-second-order model: It assumes that the adsorption rate is controlled by a chemisorption mechanism involving electron sharing or electron transfer between the adsorbent and the adsorbate [72,73]. The process is a composite adsorption reaction, which includes diffusion of the external liquid film, surface adsorption, and intraparticle diffusion [74].

$$\frac{t}{Q_t} = \frac{1}{k_2 Q_e^2} + \frac{1}{Q_e} t \quad (2)$$

The initial adsorption rate h can be calculated by using the pseudo-second-order kinetic parameters:

$$h = k_2 Q_e^2 \quad (2-1)$$

where k_2 is the pseudo-second-order adsorption rate constant ($\text{g} \cdot \text{mg}^{-1} \cdot \text{min}^{-1}$), and h is the initial adsorption rate ($\text{mg} \cdot \text{g}^{-1} \cdot \text{min}^{-1}$).

Navarathna et al. [75] adsorbed As(III) through magnetic fir biochar and the maximum removal at equilibrium was 57.8% and 68.4% at initial As(III) concentrations of 5 and 20 $\text{mg} \cdot \text{L}^{-1}$, respectively. This may be due to the adsorption of multilayered arsenite onto magnetite or the formation of a higher density of monolayer sites of arsenite at high concentrations [75]. The whole adsorption process is also consistent with the pseudo-second-order model. Similarly, Ye et al. [76] reported Fe_3O_4 /graphene composites for the elimination of As from water, with the adsorption processes all following the pseudo-second-order model. Ma et al. [77] used the arc discharge evaporation method to deposit iron catalysts on carbon electrodes and 350°C oxidation to prepare iron oxide/SWCNT composites for use as adsorbents for As in water. The kinetic data were consistent with the pseudo-second-order model, and chemisorption exists on the surface of the iron oxide particles and in the pore space [77]. Sawana et al. [78] prepared cerium oxide-coated powdered activated carbon for removal, 80% of the removal process was completed within the first 15 min, and more than 95% of both As(III) and As(V) were removed within one hour, and the adsorption process was better fitted to the pseudo-second-order model. It is found that the adsorption process of As by most renewable carbon-based materials follows the pseudo-second-order model [78]. This model can synthesize the adsorption mechanism, and the whole adsorption process includes a complex adsorption reaction including external liquid film diffusion, surface adsorption, and intra-particle diffusion, but the adsorption rate is controlled by the chemisorption mechanism [79].

Deng et al. [80] used magnetically modified activated sludge biochar to remove Sb from wastewater, and the adsorption process conformed to the pseudo-second-order model. The equilibrium adsorption increased rapidly in the first 100 min and reached equilibrium at 240 min [80]. Jia et al. [81] investigated the adsorption of Sb(III) and Sb(V) on manganese-coated biochar following the pseudo-second-order model. Sb(III) and Sb(V) were adsorbed by forming complexes with MnO_x , and some of the Sb(III) was oxidized to Sb(V), which was the predominantly adsorbed form (Fig. 8) [81]. Salam et al. [82] used multi-walled carbon nanotubes as adsorbents for Sb(III) and Liu et al. [83] used activated carbon modified by zirconium iron oxide particles for Sb(V) removal, and both of the adsorption processes investigated fitted well with the pseudo-second-order model [82,83]. Similar to the removal mechanism of As, the adsorption process of Sb by renewable carbon-based materials mostly conforms to the pseudo-second-order model, and the adsorption rate is controlled by the chemisorption mechanism.

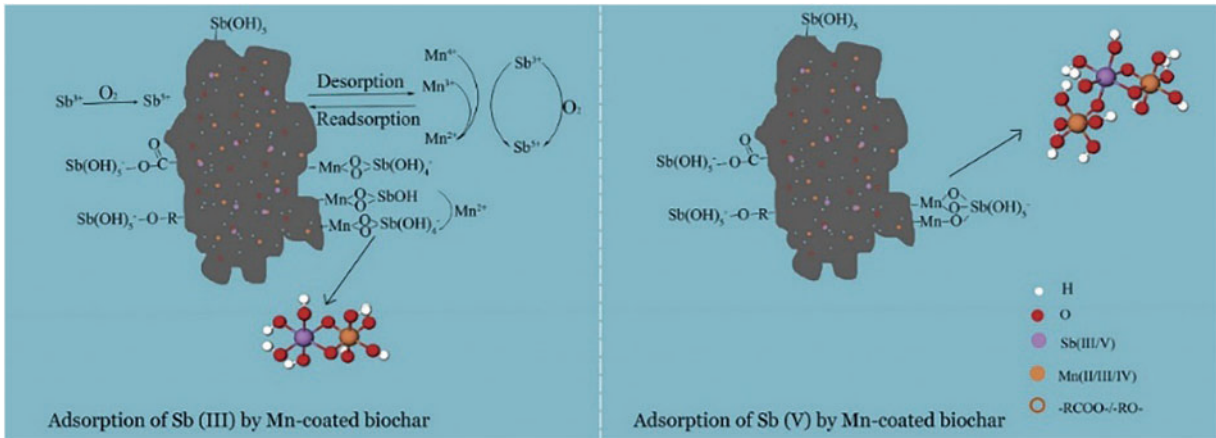


Figure 8: Schematic of the chemisorption process of Sb by manganese-coated biochar [81]. Copyright © 2020, Elsevier Ltd.

3.1.2 Adsorption Isotherm

The adsorption capacity of the adsorbent increases with the increase of the concentration of the adsorbed material and finally reaches the adsorption equilibrium. By fitting the adsorption isotherm model, the surface properties and the adsorption capacity for As and Sb of the renewable carbon-based materials can be understood in depth, which can provide theoretical basis and experimental support for the development of renewable carbon-based materials, the optimization of their application, and the industrial process. The isotherm model mainly reflects the increase in adsorption capacity with the increase in adsorbate concentration until equilibrium is reached. To better study the adsorption behavior, the common isotherm models are described as follows:

(1) Langmuir model: Ideal conditions are assumed, in which the adsorbate is increasingly adsorbed on the uniform surface of the adsorbent by the monolayer until it reaches a stable value, i.e., maximum adsorption amount [84].

$$Q_e = \frac{aQ_m C_e}{1 + aC_e} \quad (3)$$

where Q_m is the theoretical maximum adsorption capacity ($\text{mg}\cdot\text{g}^{-1}$); and a is the Langmuir equilibrium constant related to the surface heterogeneity, thus representing the adsorption strength. The essential characteristics of the Langmuir isotherm can be expressed by a dimensionless constant called separation factor (or equilibrium parameter), R_L , which is defined by [26]:

$$R_L = \frac{1}{1 + aC_0} \quad (3-1)$$

The value of R_L indicates the type of the isotherm: unfavorable ($R_L > 1$), linear ($R_L = 1$), favorable ($0 < R_L < 1$), or irreversible ($R_L = 0$).

(2) Freundlich model: It assumes that the adsorption surface is not uniform, thus the adsorption heat is unevenly distributed. The adsorption behavior of a highly heterogeneous adsorbent and the adsorption heat of the adsorption center decreases exponentially [85].

$$Q_e = K_F C_e^{1/n} \quad (4)$$

where K_F is the Freundlich adsorption capacity ($\text{mg}\cdot\text{g}^{-1}$); and n is the Freundlich constant related to the surface heterogeneity, thus representing the adsorption strength.

Mukherjee et al. [86] investigated the adsorption performance of rice straw biochar on As(V) in water, the adsorption process mainly followed the Langmuir isothermal model, and the adsorption capacity of the mono-molecular layer was $25.6 \mu\text{g}\cdot\text{g}^{-1}$. According to the model parameters, the separation factor, separation factor (or equilibrium parameter), R_L ($R_L = 0.26\text{--}0.93$), was in the range of 0–1, which indicated that the adsorption process of the biochar on As(V) adsorption by this biochar is favorable [86]. Kumar et al. [87] used manganese ferrite magnetic graphene to adsorb As(V) from water and Gallios et al. used activated carbon to remove As(V) after iron impregnation, and the adsorption processes investigated by both of them showed a better fit with Langmuir isothermal model [87,88]. In another study, the maximum adsorption of As(V) by the iron oxide/carbon nanotube composite prepared by Ma was as high as $42.30 \text{ mg}\cdot\text{g}^{-1}$ ($\text{pH} = 8$), and the adsorption isotherm was most consistent with the Freundlich model [77]. This indicates that the adsorption of As(V) on the surface of the composite belongs to multilayer adsorption, where the value of the parameter n is $8.024 > 1$. This renewable carbon-based material is favorable for As(V) adsorption [75].

Jia et al. [81] prepared manganese-coated rapeseed straw biochar for Sb removal, in which the removal was almost 100% for $10 \text{ mg}\cdot\text{g}^{-1}$ of Sb. Both Langmuir and Freundlich models fitted the adsorption process well, adsorption of Sb on this biochar was a monolayer and multilayer non-homogeneous chemisorption process. Dong et al. [89] adsorbed Sb(V) using schwertmannite/GO composites with a maximum adsorption capacity as high as $158.6 \text{ mg}\cdot\text{g}^{-1}$, and the whole adsorption process was better fitted with the Langmuir model. Liu et al. [83] reported the adsorption of Sb on nano-ferric zirconium oxide/activated carbon composites, and the Langmuir isothermal model described the adsorption process well with a maximum adsorption capacity of $11.80 \text{ mg}\cdot\text{g}^{-1}$. The process of Sb removal by renewable carbon-based materials is more consistent with the Langmuir isothermal model, and this result is consistent with the As adsorption study [89]. The adsorption process of Sb adsorption by renewable carbon-based materials is monolayer adsorption, and the adsorption properties on the surface of renewable carbon-based materials are uniform.

3.1.3 Adsorption Temperature

The effect of temperature on adsorption properties is related to the thermodynamic nature of the adsorption process, in which the parameters free energy change (ΔG), enthalpy change (ΔH), and entropy change (ΔS) can be synthesized to determine the adsorption process. The effect of temperature on the adsorption of As(V) by multi-walled carbon nanotubes in the range of 25°C – 50°C was explored by Egbosiuba et al. [90]. Based on the thermodynamic parameters, ΔG was analyzed: ΔG was negative at all times, ΔH and ΔS increased with increasing temperature, and the value of ΔH was much larger than $40 \text{ kJ}\cdot\text{mol}^{-1}$. This phenomenon has been repeatedly observed in adsorption studies of As on renewable carbon-based materials [75,89,91], which implies that the adsorption process is a spontaneous heat-trapping process controlled by chemisorption [92].

Several studies have shown that the adsorption of Sb onto renewable carbon-based materials is a spontaneous process, but both heat-absorbing and exothermic situations exist. Liu et al. [83] investigated the adsorption of Sb(V) on zirconium iron oxide-loaded activated carbon in the range of 15°C – 45°C . As the temperature increased, ΔG was always negative indicating that the adsorption process was spontaneous, while the removal of Sb(V) increased from 93.65% to 98.23%, which could indicate that it was a heat-absorbing process [83]. Deng et al. [80] similarly concluded that $\Delta G < 0$, $\Delta S > 0$, and $\Delta H > 20 \text{ kJ}\cdot(\text{mol}\cdot\text{k})^{-1}$; the adsorption of Sb(III) on magnetic $\gamma\text{-Fe}_2\text{O}_3$ -loaded biochar is a spontaneous heat-absorption process and is dominated by chemisorption (Fig. 9). Saleh et al. [91] found that the adsorption of Sb(III) on polyamide/graphene material was an exothermic process with a negative value of ΔH . This was confirmed by

Leng et al. [93] that the removal efficiency of Sb(III) by multi-walled carbon nanotubes gradually decreased with increasing temperature.

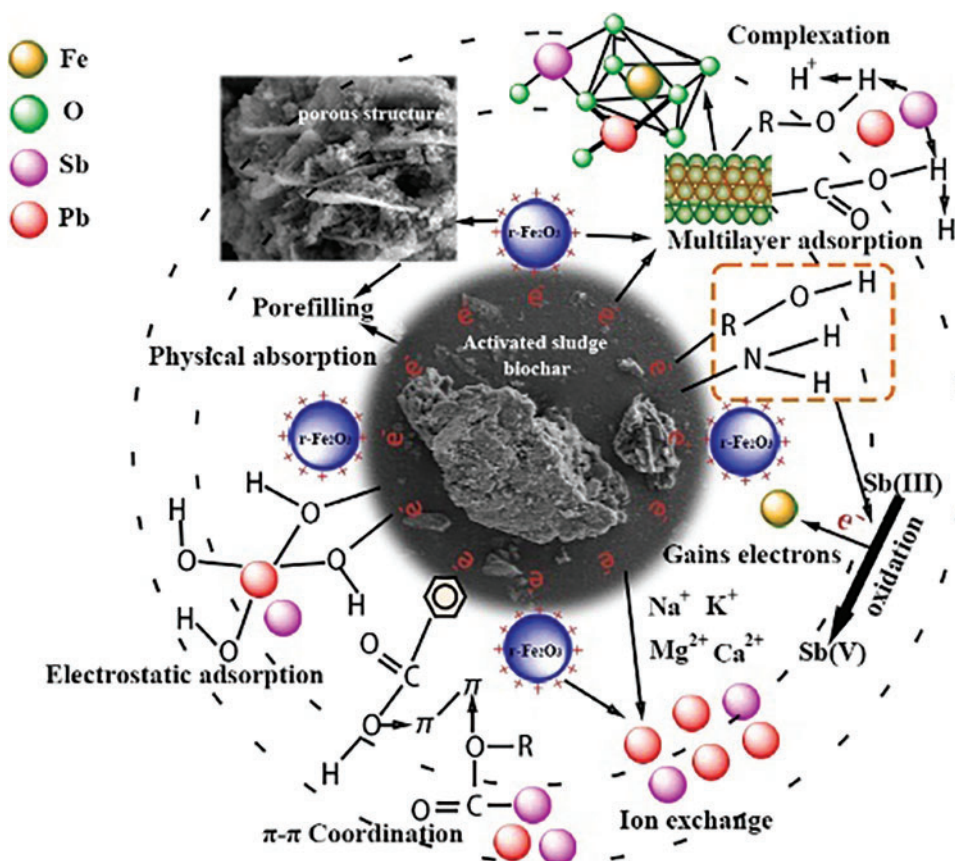


Figure 9: Schematic of chemisorption of Sb(III) by magnetic $\gamma\text{-Fe}_2\text{O}_3$ loaded biochar [80]. Copyright © 2023, Elsevier Ltd.

3.1.4 Solution pH

The pH affects the adsorption performance of renewable carbon-based materials for As and Sb through its effect on the state of existence of As and Sb in the water column or on the surface active sites of the renewable carbon-based materials, which in turn affects the adsorption performance of the renewable carbon-based materials for As and Sb. Arsenite surfaces are neutral at the same pH (6–9), so oxidation techniques are needed to convert arsenite to arsenate to enhance the ability of renewable carbon-based materials to arsenic (Fig. 10) [94]. Wang et al. [95] found that the removal of As(III) by CuFe_2O_4 composite biochar was significantly better at an initial pH of 2–6 than at an initial pH of 6–12. This may be due to the positively charged hydroxyl protonation on the surface of the biochar at low pH, which promotes the adsorption of negatively charged arsenate anions [95]. Kumar et al. [96] showed that at low pH $< \text{pH}_{\text{PZC}}$, the polar functional groups (hydroxyl, amino, carboxyl, etc.) on the surface of chitosan-GO were positively charged and enhanced the electrostatic adsorption of arsenate.

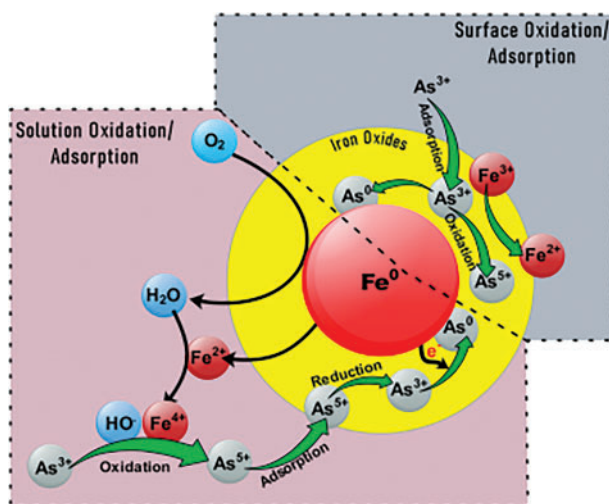


Figure 10: Schematic diagram of arsenite adsorption after oxidation [94]. Copyright © 2022, Royal Society of Chemistry

The solution pH has a large effect on the form of Sb present in water, especially Sb(III). Sb(III) is present as a neutral molecule in the pH range of 2–10.4, as $\text{Sb}(\text{OH})_4^-$ in more alkaline environments, and as $\text{Sb}(\text{OH})_2^+$ in more acidic environments [97]. Therefore, the adsorption of Sb by renewable carbon-based materials is affected by pH. Yu et al. [98] utilized FeCl_3 -modified activated carbon for the adsorption of Sb(III), and the results showed that the removal rate of Sb(III) was more than 90% at pH 5.0–9.0, and the removal rate decreased in the range of strong acid and strong base. The surface of activated carbon was negatively charged under strong alkali conditions, and the process of Fe^{3+} forming $\text{Fe}(\text{OH})_3$ colloid was weakened under strong acid conditions, which was not utilized for water purification [98]. Deng et al. [99] investigated the effect of pH on the adsorption performance of Sb(V) on amino biochar. The adsorption performance decreased but had little effect when $\text{pH} > \text{pH}_{\text{PZC}}$ (4.8), suggesting that electrostatic interaction is only one of the adsorption mechanisms of this material [99].

3.1.5 Coexisting Ion

Coexisting ions in the water column affect the adsorption properties of renewable carbon-based materials for As and Sb by competing for adsorption sites, changing the form in which the target ions exist, etc., [43,95]. Wang et al. [95] found that low concentrations of anionic NO_3^- and SO_4^{2-} ($0.001\text{--}0.1\text{ mol}\cdot\text{L}^{-1}$) in wastewater can affect the removal of As, but the effect is not significant. However, $200\text{ }\mu\text{mol}\cdot\text{L}^{-1}$ of the organic matter, sodium humate, forced a decrease in the removal of As from 98.8% to 82.9%, suggesting that the dissolved organic matter had an inhibitory effect on the removal of As from the wastewater [95]. Chen et al. [100] suggested that the coexistence of sodium humate may lead to passivation of the adsorbent and competition for adsorption with arsenic binding sites. Sawana et al. [78] similarly found that $100\text{ mg}\cdot\text{L}^{-1}$ of the anions NO_3^- and SO_4^{2-} had essentially no effect on the adsorption of As on cerium oxide-modified activated carbon. However, the same concentration of sodium dihydrogen phosphate interfered with this adsorption, with the removal of As decreasing from 90% to 18% on average [78]. Li et al. [101] suggested that this could be due to competitive adsorption due to the structural similarity between sodium dihydrogen phosphate and arsenate.

Deng et al. [80] investigated the effect of Cl^- , CO_3^{2-} , and PO_4^{3-} anions and cations such as Na^+ and Ca^{2+} on the removal of Sb(III) from wastewater by magnetic $\gamma\text{-Fe}_2\text{O}_3$ -loaded biochar. Cations and Cl^- had little effect on the adsorption effect, whereas CO_3^{2-} and PO_4^{3-} formed complexes with surface iron ions and competed with Sb(III) for active sites, thus reducing the adsorption effect [80]. The inhibitory effect of PO_4^{3-} on the removal of Sb(III) and Sb(V) from water by renewable carbon-based materials was also demonstrated by Mishra et al. [102].

3.1.6 Influence of Material Properties on the Adsorption Process

First of all, most research reports on the surface modification of renewable carbon materials initially aim to improve the original rugged structure, enhance its surface functionality, or change the surface charge. This will further promote the adsorption performance of carbon materials, enhance the selective adsorption of pollutants, and improve the adsorption kinetics and thermodynamic processes [79,81]. For example, functional groups such as carboxyl groups ($-\text{COOH}$) and amino groups ($-\text{NH}_2$) are introduced on the surface of renewable carbon materials [23,83]. These functional groups can provide additional adsorption sites and enhance interactions with arsenic and antimony. These functional groups usually form coordination bonds with arsenic and antimony ions through charge transfer, enhancing adsorption [5,20,80]. Moreover, the polarity of the functional groups makes the carbon material more hydrophilic in water, which helps to improve its contact with pollutants in water. On the other hand, doping with metal ions such as Fe and Mn can change the electronic structure and surface properties of the carbon material, enhancing its adsorption capacity for arsenate and antimonate anions [88,89]. Additionally, metal ions can form complexes with arsenic and antimony, reducing the activation energy of the reaction and thus helping to promote the removal of arsenic and antimony.

3.2 Discussion of the Forms of Existence and Adsorption Processes of Arsenic and Antimony

In natural water bodies, dissolved arsenic mainly exists in the form of arsenite As(III) , arsenate As(V) , or methylated arsenic compounds. Groundwater (with a pH of 6.5–8.5) is often anaerobic, and arsenic mainly exists in the form of the neutral molecule H_3AsO_3 [3,103]. It is difficult to remove arsenic by electrostatic adsorption or complexation with an adsorbent. Specifically, under acidic conditions ($\text{pH} < 7$), arsenic mainly exists in the form of As(III) (As^{3+} , e.g., arsenic acid). As(OH)_2^+ ions may also form. In neutral to slightly alkaline conditions ($\text{pH} 7\text{--}9$), it is mainly present as As(V) (As^{5+} , e.g., arsenate ions H_2AsO_4^- and HAsO_4^{2-}). In alkaline conditions ($\text{pH} > 9$), arsenic is mainly present as HAsO_4^{2-} and AsO_4^{3-} . During conventional adsorption treatment, As(III) is often oxidized to As(V) under certain conditions, and As(V) is used to adsorb and remove it due to its electronegativity in water [11,103]. Usually, As(III) is more toxic than As(V) . The equilibrium distribution of the ionic forms of As(III) and As(V) in solution are shown in Fig. 11a and b, respectively. Additionally, there are two main types of reports on the effects of interfering ions. Some cations (e.g., Ca^{2+} , Mg^{2+}) and anions (e.g., Cl^- , SO_4^{2-}) can affect the solubility and chemical form of arsenic. In the presence of high concentrations of interfering ions, the solubility of arsenic may decrease and precipitation may form. Sulfides (e.g., HS^-) can react with arsenic under acidic conditions to form arsenide precipitates (e.g., As_2S_3), thereby reducing its concentration in water [103].

Antimony is mainly found in water bodies in the +3 and +5 oxidation states. According to the thermodynamic data and $\phi\text{--pH}$ plot, antimony in neutral, oxygen-rich surface water usually exists in the +5 valence state as Sb(OH)_6^- [89,104]. As the water depth increases, the proportion of Sb(V) in total antimony gradually decreases. In anoxic environments, most antimony exists in the +3 valence state as Sb(OH)_3 . In the presence of sulfur, Sb_2S_3 or SbS_2^- is formed. However, many studies have found that Sb(V) also exists in hypoxic water bodies, while Sb(III) is also detected in oxygen-rich water bodies, suggesting that the

valence state of antimony in water bodies and its redox reactions are affected by many factors [19,83,105]. Sb(III) exists as a neutral molecule ($\text{Sb}(\text{OH})_3$, $\text{SbO}(\text{OH})$, or HSbO_2) over a wide pH range (approximately 2 to 10). In an environment with strong acid, is SbO^+ or $\text{Sb}(\text{OH})_2^+$, while it is SbO_2^- or $\text{Sb}(\text{OH})_4^-$ in a strongly alkaline environment. Free Sb^{3+} can only exist in an extremely acidic environment. Sb(V) exists in the form of $\text{Sb}(\text{OH})_6^-$ or SbO_3^- in the weak acid, neutral, and alkaline ranges, and as SbO_2^- in strong acid conditions [102,105]. The ionic distribution diagrams for Sb(III), Sb(V), and the main chemical forms of Sb in water are shown in Fig. 11c. Additionally, some high concentrations of cations and anions (e.g., Ca^{2+} , Mg^{2+} , SO_4^{2-}) may cause antimony to precipitate or form complexes [104,105].

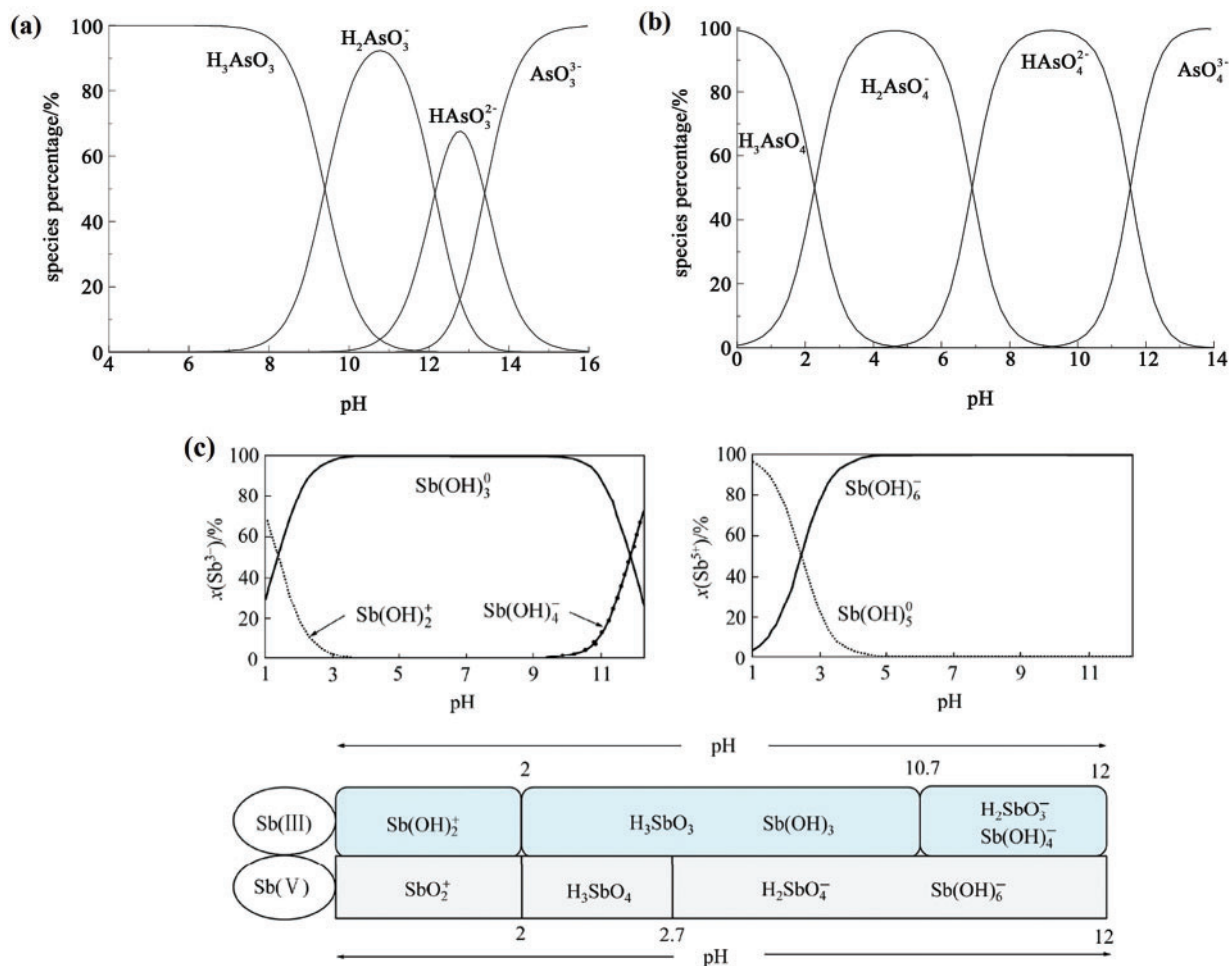


Figure 11: (a) Equilibrium distribution of As(III) species in aqueous with a total As(III) concentration of $500 \text{ mg}\cdot\text{L}^{-1}$ [103], (b) Equilibrium distribution of As(V) species in aqueous with a total As(V) concentration of $500 \text{ mg}\cdot\text{L}^{-1}$ [103], (c) the ion distribution diagrams of Sb(III) and Sb(V) and the main chemical forms of Sb in water [104,105]. Refs. [103,104] Copyright © 2022, CNKI, China Academic Journal Electronic Publishing House. And Ref. [105] Copyright © 2017, Elsevier Ltd.

3.3 Adsorption Mechanisms

The adsorption process of anionic heavy metals such as As and Sb by renewable carbon-based materials involves various mechanisms such as physical adsorption, ion exchange, electrostatic interactions, and

surface complexation (Fig. 12) [106]. The strength of action of each mechanism depends on the surface chemistry of the adsorbent, the ionic environment, and the nature of the contaminant.

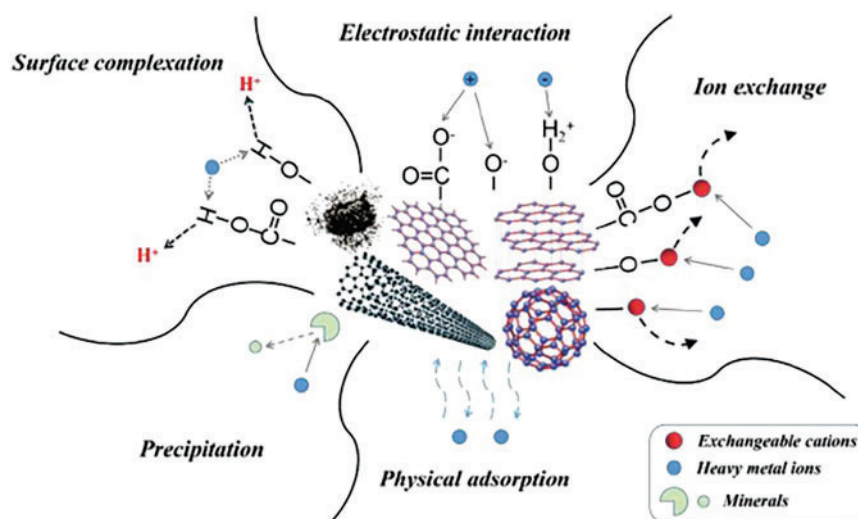


Figure 12: Schematics of adsorption mechanisms of heavy metals onto carbon-based materials [106]. Copyright © 2019, Elsevier Ltd.

3.3.1 Physical Adsorption

Physical adsorption is the process by which As and Sb diffuse into the pores of renewable carbon-based material and are then immobilized on the surface of the material. This process does not form chemical bonds and is mainly influenced by the pore size distribution and surface area of the adsorbent. Physical adsorption is the most common adsorption process, which can be enhanced by improving the pore size distribution and specific surface area of the adsorbent. The surface area increases through the increase of micropores to promote physical adsorption, while the increase of mesopores can accelerate the diffusion of contaminants [106]. By loading iron hydroxide nanoparticles onto activated carbon, Nieto-Delgado et al. [107] both enhanced the active surface area of activated carbon and effectively avoided the clogging of activated carbon pores to promote the physisorption of As(V) (Fig. 13). Deng et al. [80] determined the specific surface area and pore volume of graphene oxide composites to be $77.924 \text{ m}^2 \cdot \text{g}^{-1}$ and $0.210 \text{ cm}^3 \cdot \text{g}^{-1}$, respectively, with an average BJH pore size of 1.190 nm, and the large pore size of this material promotes the physisorption of Sb.

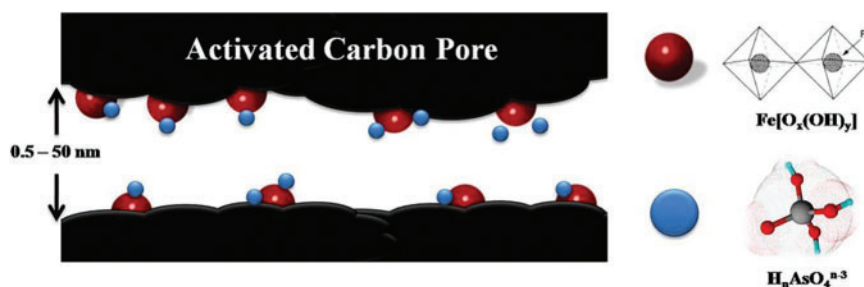


Figure 13: Schematic diagram of physisorption of As(V) on loaded biochar [107]. Copyright © 2012, Elsevier Ltd.

3.3.2 Ion Exchange

Ion exchange refers to the adsorption mode in which the anions As and Sb in water are exchanged with the functional groups of the renewable carbon-based material or surface ions. The adsorption effect of this action mainly depends on the ionic size of the pollutant and the surface functional groups of the adsorbent [108]. Luo et al. [109] investigated the adsorption performance and X-ray Photoelectron Spectroscopy (XPS) of titanium-modified ultrasonic biochar on As(V). The results of adsorption kinetics fitted well with the pseudo-second-order model, indicating that the adsorption process was dominated by chemical reactions, such as ion exchange and surface complexation. XPS spectra showed a decrease in Ti(IV) content after adsorption and the appearance of the characteristic peaks of As(V), which indicated that there was a Ti-As ion exchange on the surface of the adsorbent during the adsorption process. In the adsorption of Sb(V) using zirconium iron oxide-loaded activated carbon, Liu et al. [83] found that in an acidic environment, the material is positively charged by protonation, and Sb(V) is adsorbed by ion exchange or electrostatic interactions. Under alkaline conditions, electrostatic interactions were negligible and the adsorption process was controlled only by ion exchange [83].

3.3.3 Electrostatic Interaction

Electrostatic interactions are fundamental to the creation of ionic bonds, encompassing both electrostatic attraction and repulsion [110]. The adsorption process between the positively charged renewable carbon-based materials on the surface and the anions As and Sb can be enhanced by electrostatic adsorption, which is mainly affected by the solution pH and the zero-charge point of the renewable carbon-based materials [97]. Sattar et al. [111] found that the O=C-O and C=O intensity on the surface of peanut shell biochar weakened after the adsorption of As(III) and As(V) by Fourier Transform Infrared Spectrometer (FTIR) and XPS analyses and that electrostatic interactions were the main mechanism for the adsorption of As(III)/As(V) by this material. Lingamdinne et al. [112] used iron oxide-graphene oxide-gadolinium oxide composites to adsorb As(V), and the adsorption varied with pH and ionic strength, confirming that the adsorption process was caused by electrostatic interaction and surface complexation (Fig. 14). Liu et al. [83] reported the synthesis of activated carbon composites loaded with zirconium iron oxide (ZIC) nanoparticles for the removal of Sb(V) from water. The removal of Sb(V) by ZIC was 97.35%–97.82% when the pH was 4–5; however, the adsorption capacity gradually decreased with the increase in pH [83]. This was mainly because Sb(V) mainly existed in aqueous solution as H_2SbO_4^- and $\text{Sb}(\text{OH})_6^-$, and there was competition between the increase of hydroxyl groups and hydroxides and Sb(V) under alkaline conditions. The phenomenon illustrates the reverse side of the electrostatic interaction between Sb(V) and the adsorbent.

3.3.4 Surface Complexation

The complexes formed by surface complexation (inner and outer spheres) have unique metal-functional group interactions that play a major role in the adsorption of As and Sb on renewable carbon-based materials [113]. Sattar et al. [111] utilized peanut shell biochar for the adsorption of As(III) and As(V) from water and showed that the surface active sites influenced the rate of adsorption, which may involve surface complexation between As anions and surface functional groups. Shaikh et al. [114] combined FTIR to analyze the surface features of zero-valent iron nano-loaded biochar, which mainly contained N-H, C=O, and C-O, which were able to form strong hydrogen bonds and surface complexes with As(III) and As(V) oxygenated anions (Fig. 15). Deng et al. [80] found that Sb(III) and Sb(V) bind to Fe-OH on magnetic $\gamma\text{-Fe}_2\text{O}_3$ -loaded biochar to create Fe-O-Sb bonds and enhance the adsorption process. This finding was confirmed in the study by Cheng et al. (Fig. 16) [115]. Li et al. [116] used phosphogypsum-modified lees biochar to remove

Sb(V) from water, and Ca-O-Sb complexes were formed on the surface of the material by FTIR and XPS analysis before and after adsorption.

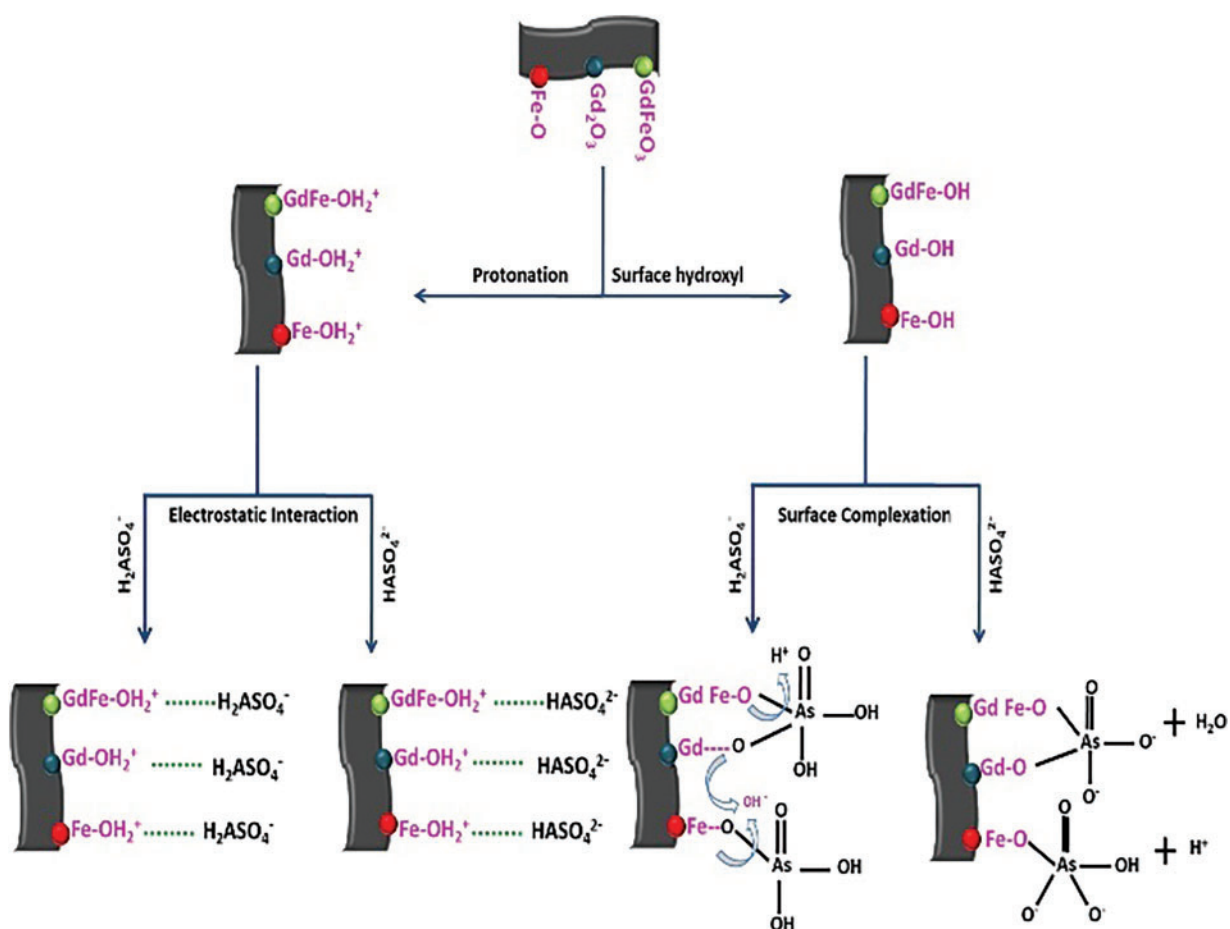


Figure 14: Mechanism schematic of As(V) adsorption by composite graphene oxide [112]. Copyright © 2020, Elsevier Ltd.

Overall, the adsorption process of anionic heavy metals, such as As and Sb, by renewable carbon-based materials mainly consists of physical adsorption, ion exchange, electrostatic interactions, and surface complexation, with the latter two actions being the main adsorption mechanisms. To effectively remove As(III), which is difficult to remove, the renewable carbon-based materials are often modified by iron oxides and other oxides, and the complexation is strengthened to promote the combination of As(III) into arsenic-iron compounds and the oxidation of As(V), which is less toxic (Fig. 17) [95]. The removal of Sb(III) from some renewable carbon-based materials is accompanied by redox reactions because Sb(III) is easily oxidized to Sb(V) [117,118].

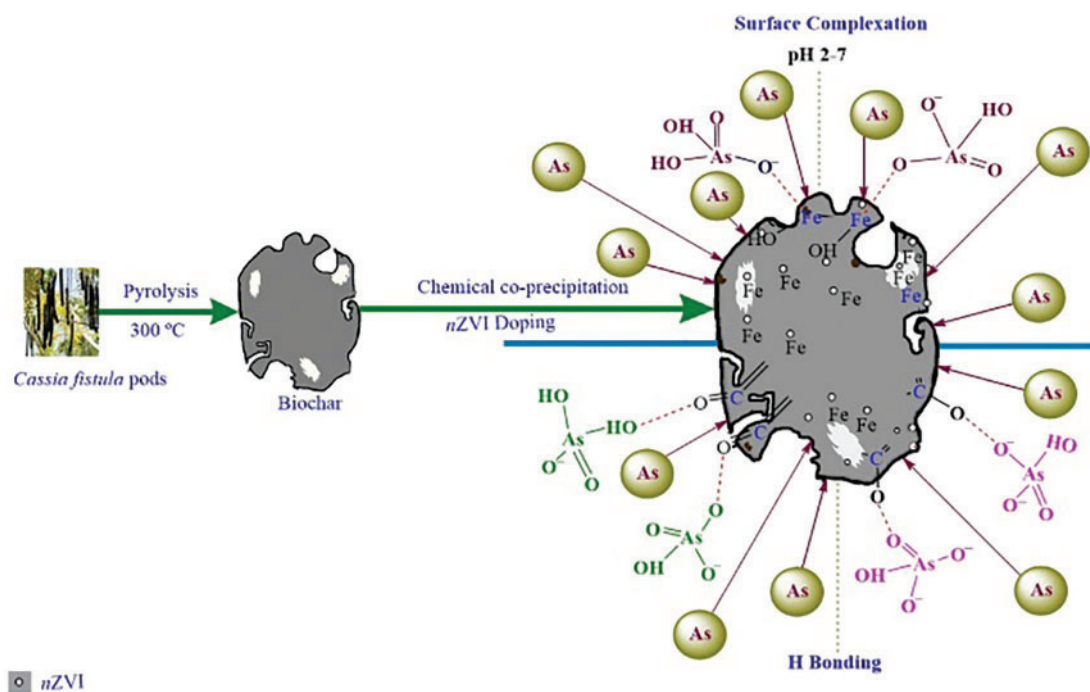


Figure 15: Adsorption mechanisms of modified biochar for As(III) and As(V) removal [114]. Copyright © 2020, Elsevier Ltd.

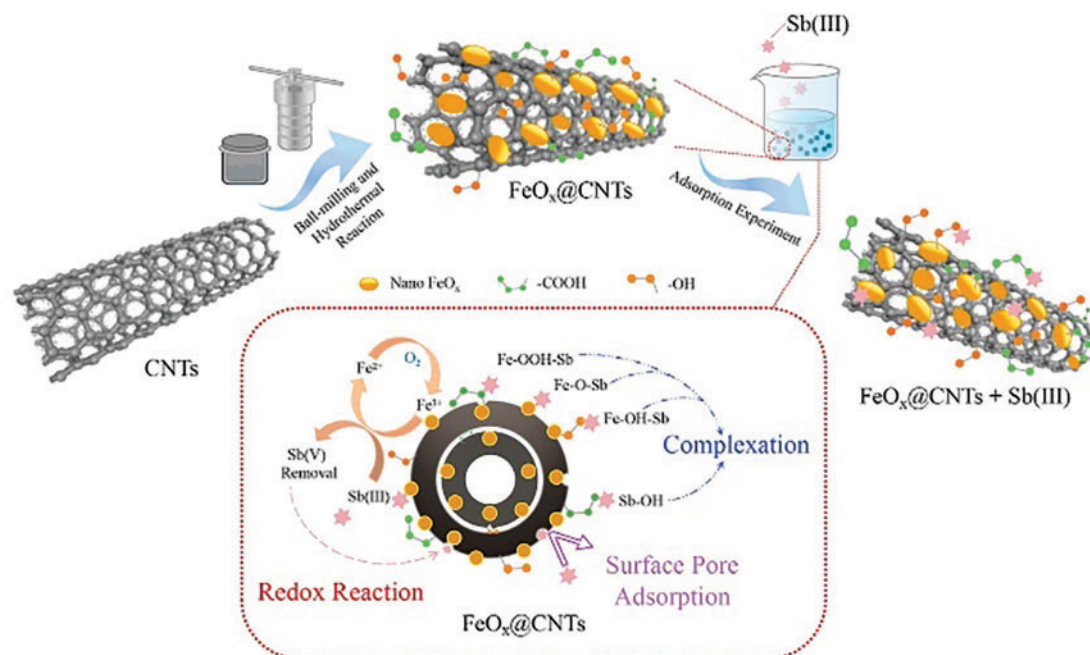


Figure 16: Schematic of the adsorption mechanisms of Sb(III) by magnetic iron-modified carbon nanotube composites [115]. Copyright © 2022, Elsevier Ltd.

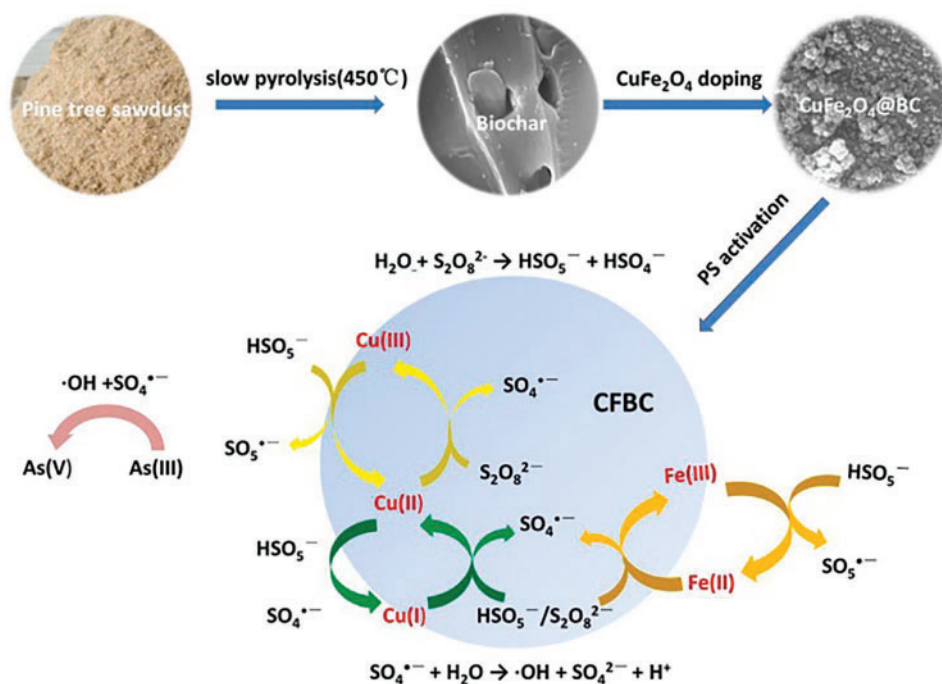


Figure 17: Removal of As(III) by oxidative complexation of the copper ferrite@biochar [95]. Copyright © 2023, Elsevier Ltd.

4 Comparison of the Adsorption Capacity of Renewable Carbon-Based Materials and Potential Challenges

4.1 Comparison of the Adsorption Capacity

Statistical reports of adsorption of As and Sb by different renewable carbon-based materials are shown in Tables 2 and 3, respectively. The adsorption process of As on renewable carbon-based materials mostly conforms to the pseudo-second-order kinetic model and Langmuir isothermal model, which proves that the adsorption process is a single-molecule adsorption process dominated by chemical adsorption, and electrostatic interactions and surface complexation are the main adsorption mechanisms. As(III) and As(V) exist in different forms at different pH ranges, with the arsenite surface being neutral at the same pH (6–9). The optimal pH for the adsorption of As(III) by most renewable carbon-based materials is between 6 and 7, while the optimal pH for the adsorption of As(III) is between 3 and 6 [114]. The pseudo-second-order kinetic model and the Langmuir/Freundlich isothermal adsorption model were able to better fit the adsorption process of most renewable carbon-based materials for Sb. This suggests that the adsorption process is also chemisorption-dominated, which includes effects such as electrostatic interactions and surface complexation, and there is also an oxidation of Sb(III) to Sb(V) (Fig. 18) [119].

Table 2: Comparison of as adsorption properties of different renewable carbon-based materials

Adsorbent	Heavy metals	Optimal isotherm model	Optimal kinetic model	Optimal adsorption conditions			Average pore size (nm)	Specific surface area (m ² ·g ⁻¹)	Maximum adsorption capacity (mg·g ⁻¹)	Ref.
				Adsorbent concentration (mg·L ⁻¹)	Time	Temp. (°C)				
Magnetite-Douglas fir biochar	As(III)	-	Pseudo-second-order	-	1-1.5 h	25	-	320.1	5.49	[75]
Nanometer iron oxide-SWCNT	As(V)	Freundlich	Pseudo-second-order	-	3 min	-	-	-	49.65	[77]
Ceria-activated carbon	As(III)/As(V)	Freundlich	Pseudo-second-order	100	15 min	25	-	635	10.3/12.2	[78]
Rice straw-derived biochar	As(V)	Langmuir	Pseudo-second-order	200	2 h	-	2.8-3.5	133	25.6 µg	[86]
GO-MnFe ₃ O ₄	As(III)/As(V)	Langmuir	-	200	-	-	7.5	196	146/207	[87]
Magnetic Manganese Oxides-AC	As(V)	Langmuir	-	-	-	25	1.7-2	686	19.35	[88]
Chitosan functionalized GO	As(III)/As(V)	Langmuir	Pseudo-second-order	1	60 min	-	-	-	64.2/71.9	[96]
PEG/MWCNT	As(III)	Koble-Corrigan	Parabolic or Weber-Morris model	100	60 min	25	17.4	22.5	13.3	[92]
Iron hydro(oxide) nanoparticles-AC	As(V)	Freundlich	Pseudo-second-order	-	-	25	34 ± 5	857	3.25	[107]
Peanut shell biochar	As(III)/As(V)	Langmuir	Pseudo-second-order	0.6	2 h	-	-	-	-	[111]
Fe-GO-Gd	As(V)	-	-	0.7	187 min	-	6.68	138.2	-	[112]
Iron nanocomposite-biochar	As(III)/As(V)	Langmuir	Pseudo-second-order	-	-	-	7-32	-	0.24/0.25	[114]
Magnetic hyacinth biochars	As(III)/As(V)	Langmuir-Freundlich	Pseudo-second-order	-	-	-	-	69	7.41	[120]
Iron oxide-modified GO	As(III)/As(V)	Freundlich	Pseudo-kinetic model	180	24 h	25	2.497	50 nm	54.18/26.76	[121]

(Continued)

Table 2 (continued)

Adsorbent	Heavy metals	Optimal isotherm model	Optimal kinetic model	Optimal adsorption conditions			Average pore size (nm)	Specific surface area (m ² ·g ⁻¹)	Maximum adsorption capacity (mg·g ⁻¹)	Ref.
				Adsorbent concentration (mg·L ⁻¹)	Time	Temp. (°C)				
GO-manganese	As(V)	Langmuir	Pseudo-second-order	1	48 h	-	4	150.42	102	[122]
Magnetic iron oxide-CNTs	As(III)/As(V)	Langmuir	Pseudo-second-order	-	60 min	25	7	209.8	24.04/47.41	[123]
MWCNT-ZrO ₂	As(III)/As(V)	Langmuir-Freundlich	Pseudo-second-order	-	-	-	6	152	2/5	[124]
Iron-chemical AC	As(V)	-	-	-	-	25	7	1266	1.32	[125]
Iron-modified activated carbon	As(III)/As(V)	Langmuir	Parabolic diffusion equation	-	12 h	-	6	-	38.8/51.3	[126]

Note: Please note that a “-” indicates a default or undetermined value. Specific surface area usually refers to the Brunauer-Emmett-Teller model calculated BET specific surface area or Langmuir specific surface area.

Table 3: Comparison of Sb adsorption properties of different renewable carbon-based materials

Absorbent	Heavy metals	Optimal isotherm model	Optimal kinetic model	Specific surface area ($\text{m}^2 \cdot \text{g}^{-1}$)	Maximum adsorption capacity ($\text{mg} \cdot \text{g}^{-1}$)	Ref.
MWCNTs	Sb(III)	–	Pseudo-second-order	89.2	0.325	[82]
Nano zirconium iron oxide-AC	Sb(V)	Langmuir-Freundlich	Pseudo-second-order	23.989	11.8	[83]
GO-SCH	Sb(V)	Langmuir	–	287.6	158.6	[89]
Polyamide-graphene	Sb(III)	Langmuir	Pseudo-second-order	421	158.2	[92]
Graphene	Sb(III)	Langmuir-Freundlich	Pseudo-second-order	154.43	10.919	[93]
FeCl_3 -AC	Sb(III)	Freundlich	Pseudo-frist-order	940.03	2.64	[98]
NMSH-BC	Sb(V)	Langmuir-Freundlich	Pseudo-second-order	91.8	241.92	[99]
CNT-Fe(0)	Sb(III)/Sb(V)	Langmuir	Pseudo-second-order	132	250	[102]
FeO_x @CNTs	Sb(III)	Redlich-Peterson	Pseudo-second-order	242	172	[115]
La-doped magnetic biochars	Sb(V)	Langmuir	Pseudo-second-order	287.11	18.92	[127]
BC@MF	Sb(III)	Freundlich	Pseudo-second-order	–	77.44	[128]
Fe-CMB	Sb(V)	Langmuir	Pseudo-second-order	–	58.3	[129]
CIB300	Sb(III)	Langmuir-Freundlich	Pseudo-second-order	3.46	16.1	[130]
FeCl_3 BC900	Sb(III)/Sb(V)	Langmuir	Pseudo-second-order	520	1.9/17.6	[131]
nZVI-BC	Sb(III)	Langmuir-Freundlich	Pseudo-second-order	122.27	98.25	[132]
β -FeOOH/BC	Sb(III)	Langmuir	Pseudo-second-order	–	202.53	[133]
S-nZVI@GO	Sb	Langmuir-Freundlich	Pseudo-second-order	–	311.75	[134]

Note: Please note that a “-” indicates a default or undetermined value. Specific surface area usually refers to the Brunauer-Emmett-Teller model calculated BET specific surface area or Langmuir specific surface area.

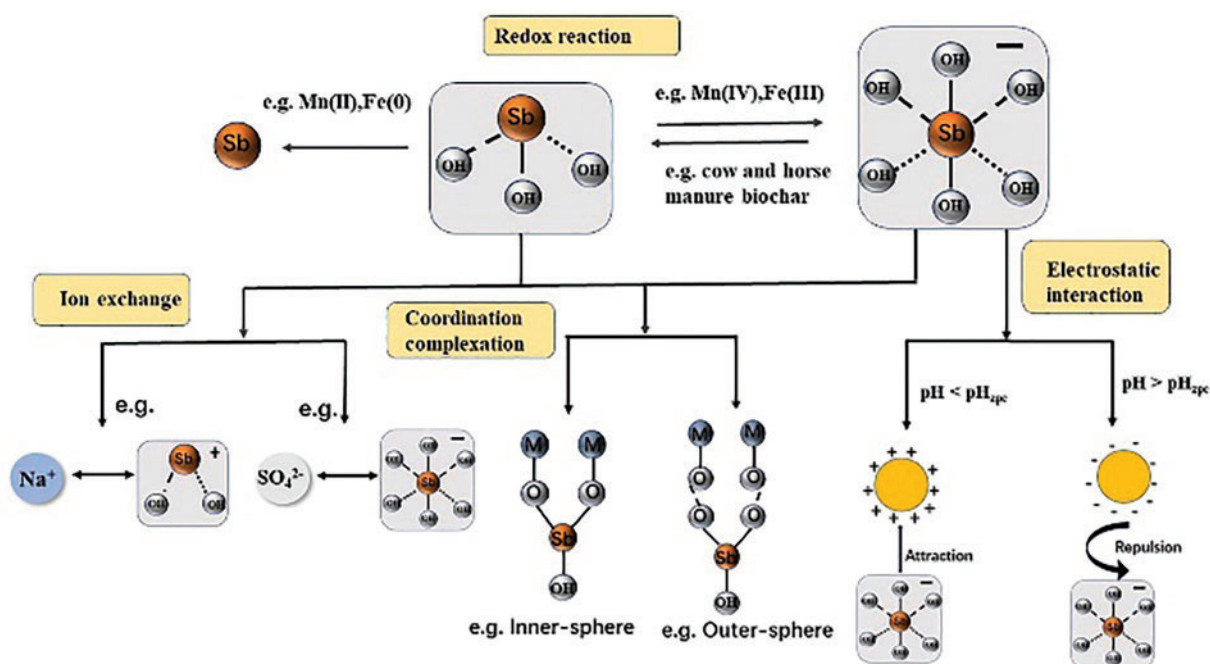


Figure 18: Possible removal mechanisms of Sb(III) and Sb(V) based on their respective chemical properties [119]. Copyright © 2023, Elsevier Ltd.

Usually, the properties of the material (e.g., pore size, and specific surface area) significantly affect the adsorption performance of As and Sb [43]. A larger specific surface area and a more abundant pore volume, as well as a suitable mesoporous or microporous structure, can all help to increase the adsorption capacity for As and Sb. Specifically, biochar-based materials generally have a porous structure with a wide pore size distribution, mainly mesopores and micropores. They have a relatively high specific surface area (usually 50–500 m²·g⁻¹) [27]. The surface is rich in functional groups such as carboxyl groups and phenolic hydroxyl groups [26]. These synergies enhance the interaction of the biochar-based material with arsenic and antimony in water, and are particularly suitable for removing As³⁺ and Sb³⁺ from water, owing to the formation of coordination bonds. Biochar-based materials are suitable for a wide range of different forms of arsenic and antimony and perform particularly well in natural environments. Graphene usually does not have a significant pore structure and mainly exists in two-dimensional planes with small pore sizes [30]. Graphene has a very high specific surface area (up to 2630 m²·g⁻¹), but it may be affected by agglomeration in practical applications [50], which limits the liquid phase diffusion of ions. If appropriate functional groups are introduced during modification, their adsorption capacity for arsenic and antimony can be significantly improved. Graphene oxide has a certain porous structure, a large specific surface area (500–1000 m²·g⁻¹), and the surface contains various oxidation groups, such as carboxyl groups, which give it good selectivity and efficiency in removing arsenic and antimony [76]. Graphene-like materials have great potential for the removal of arsenic and antimony, but practical applications may require modification to improve their affinity. Carbon nanotubes have small pore sizes, typically in the nanometer range, and a unique tubular structure. Their specific surface area is high (up to 1000 m²·g⁻¹), but depends on the specific structure and arrangement [77,82]. The high specific surface area and unique pore size of carbon nanotubes make them highly adsorptive for arsenic and antimony under certain conditions. However, the introduction of functional groups through surface modification can further improve their selective adsorption of arsenic and antimony [90]. Activated carbon is similar to biochar and has a porous structure, containing micropores and

mesopores, which are suitable for adsorbing smaller molecules [107]. It usually has a large specific surface area ($500\text{--}1500\text{ m}^2\cdot\text{g}^{-1}$) and a variety of surface functional groups. It is often used in water treatment to remove arsenic and antimony [126].

4.2 Potential Challenges and Solutions

There is great potential for the use of renewable carbon materials in the removal of arsenic and antimony from water, but there are some influencing factors and obstacles in practical applications. These mainly include: (1) The basic properties of carbon materials. The specific surface area and pore structure of renewable carbon materials are crucial to their adsorption capacity [135]. A larger specific surface area can help to improve the adsorption capacity for arsenic and antimony, while the size and distribution of the pore size can also affect the selective adsorption of molecules of different sizes. Functional groups on the surface of the carbon material (e.g., carboxyl groups) can affect the interaction with arsenic and antimony. Some functional groups may enhance adsorption, while others may inhibit the adsorption process [136]. Regenerated carbon materials must maintain a certain degree of physical and chemical stability during water treatment to prevent decomposition or the release of other harmful substances during the treatment process [137]. (2) Water environmental conditions. The pH of the water affects the form in which arsenic and antimony are present, and thus their adsorption capacity on the renewable carbon material. The chemical forms of arsenic and antimony are different under different pH conditions, which may lead to changes in adsorption efficiency. Specifically, the coexisting cations (such as Ca^{2+} , etc.) and anions (such as SO_4^{2-} , etc.) in the wastewater may compete with arsenic and antimony for adsorption. The higher the concentration of competing ions, the more likely it is to occupy the active sites of the carbon material, thereby reducing the adsorption of arsenic and antimony [138]. Organic matter in wastewater (such as phenols and dyes) can attach to the surface of the carbon material to form a covering layer, preventing arsenic and antimony from contacting and adsorbing. The coexisting ions and organic matter in wastewater may cause changes in the pH of the aqueous phase, altering the form of arsenic and antimony and affecting their solubility and adsorption characteristics [103,104]. Additionally, the presence of some impurities may physically prevent the solutes from contacting these adsorption materials, reducing their overall adsorption efficiency. (3) Material recyclability. The preparation process of renewable carbon materials and the selection of regeneration technology need to be reasonably designed to ensure that the performance after regeneration can be restored to the initial state [135]. However, due to the repeated use of these materials in wastewater treatment, their physical and chemical properties may be affected, especially their adsorption performance may be reduced. Therefore, it is necessary to achieve the goal of long-term stability and reusability through some regeneration technologies to achieve economic benefits. These common regeneration techniques include: thermochemical methods, microwave methods, ultrasonic methods, electrochemical methods, photocatalysis, biological regeneration, etc., as well as coupling techniques of these methods [139]. (4) Cost and economy. The production cost of renewable carbon materials and the energy consumption of the regeneration process are important factors affecting their large-scale application. Excessive costs may limit their use. The treatment efficiency of arsenic and antimony removal must be balanced with economy to ensure that the water treatment process is not only effective but also feasible and economical [140]. (5) Potential environmental risks and application safety. When applying renewable carbon materials, their environmental impact must be considered, including possible secondary pollution and the potential impact on water bodies after material degradation. It is crucial to ensure that the materials do not release toxic substances during the water treatment process or endanger human health [141]. In summary, renewable carbon materials have the potential for the removal of arsenic and antimony from water, but there are many influencing factors and potential obstacles that need to be considered in practical applications. Optimizing material properties, adjusting water quality parameters,

designing effective regeneration processes, and assessing economic and environmental impacts are the keys to their effective application.

Possible strategies to mitigate these impacts include: (a) Selecting appropriate renewable carbon materials. Select carbon materials with high specific surface area and appropriate pore size to improve the adsorption capacity for target pollutants, and combine with modification techniques (such as introducing functional groups, metal doping, etc.) to enhance the selective adsorption of arsenic and antimony [137]. (b) Optimize the wastewater treatment process. Optimize the existence form of arsenic and antimony by adjusting the pH value of the aqueous phase to improve their adsorption on the surface of the carbon material [22,50]. Moreover, under acidic conditions, the cationic forms of arsenic and antimony are more easily adsorbed. In addition, the total ion concentration in the water can be adjusted to reduce the impact of competitive adsorption. (c) Pretreatment of wastewater or coupling with other water treatment technologies. Pretreatment of actual wastewater is carried out to remove high concentrations of coexisting ions or organics, reducing interference with the subsequent adsorption process. In addition, coupling with other water treatment technologies (such as flocculation, sedimentation, membrane separation, etc.) can also be considered to remove most of the interfering substances first, and then selectively remove arsenic and antimony in the wastewater [90,110]. Finally, in the actual wastewater treatment, real-time monitoring of the water quality is also required to evaluate the impact of different coexisting ions and organic matter on the adsorption efficiency of the carbon material, so that effective adjustments can be made at any time. (d) The adsorbent material should be regularly regenerated to remove the interfering substances that have been adsorbed and restore their adsorption capacity [138,140]. An appropriate regeneration process should be selected to ensure that the performance of the material is maintained after regeneration. Through the above measures, these effects or limitations can be effectively mitigated, and the removal efficiency of arsenic and antimony in wastewater treatment can be improved. The application of these strategies needs to be considered comprehensively based on the specific wastewater characteristics and treatment goals.

5 Conclusions and Research Outlook

Biochar, graphene, carbon nanotubes, and activated carbon are four typical renewable carbon-based materials. For the adsorption of As and Sb by renewable carbon-based adsorbents, the pseudo-second-order tends to fit the adsorption process better than other models, and Langmuir and Freundlich's isothermal models can fit the adsorption process better. Surface complexation and electrostatic interactions are the main mechanisms of the adsorption process.

Biochar has better adsorption performance but poor stability and is easy to agglomerate; activated carbon has high adsorption efficiency for both but is more affected by pH. Graphene or carbon nanotube materials loaded with Fe-Mn oxides are structurally stable and have a large specific surface area, which not only adsorb As and Sb well, but also overcomes the effect of pH while weakening the agglomeration of Fe-Mn oxides. The adsorption process also makes full use of the complexation and oxidizing properties of ferromanganese oxides. In the future development direction, this composite new nanoscale renewable carbon-based adsorbent material has a large development potential. However, the loading process of Fe-Mn oxides on novel renewable carbon-based nanomaterials is relatively cumbersome and time-consuming; moreover, the research on such materials is still in the experimental stage, and static adsorption experiments have been used in general studies. The experimental study mainly focuses on the examination of adsorption performance and influencing factors, including adsorption kinetics and mechanisms. There are fewer studies on the column adsorption of flow type, and the dynamic experiment of flow type is closer to the adsorption treatment of pollutants in the actual wastewater, and the experimental results can provide process parameters

for the actual treatment engineering of this type of wastewater, as well as evaluating the service life of the composite adsorption materials and so on.

Future research in the adsorption of As and Sb from wastewater by renewable carbon-based materials could start from the following aspects:

(1) Design of multifunctional composites: The design and synthesis of multifunctional composites can be further explored to introduce more functional groups or nanostructures to improve the adsorption performance and selectivity, and at the same time to realize the efficient removal of As and Sb.

(2) Adsorption mechanism research: In-depth study of the adsorption mechanism of renewable carbon-based materials on As and Sb, including surface chemical reactions, adsorption kinetics, and thermodynamic properties, etc., to provide a theoretical basis for further optimization of the adsorption process.

(3) Regeneration and recycling: Develop efficient regeneration technologies to realize the recycling of renewable carbon-based materials, reduce the cost and waste of resources in the process of wastewater treatment, and at the same time reduce the impact on the environment.

(4) On-site application and engineering: apply renewable carbon-based materials to actual wastewater treatment projects and carry out on-site tests and application demonstrations to verify their effectiveness and feasibility in large-scale applications and promote their industrialization and commercialization.

(5) Environmental risk assessment: Conduct a comprehensive environmental risk assessment of the application of renewable carbon-based materials in wastewater treatment, including the ecotoxicity of the materials and the environmental behavior of the degradation products, etc., to ensure that they will not adversely affect the environment and the ecosystem in practical application.

The above research will promote greater progress in the adsorption study of As and Sb by renewable carbon-based materials, provide more effective technical support and solutions for solving the problem of wastewater pollution, and is expected to become one of the important technological means in the field of environmental governance in the future.

Acknowledgement: None.

Funding Statement: This research was funded by the following grants, including the Key Research and Development Program of Shaanxi Province (Nos. 2023-LL-QY-42, 2024NC-ZDCYL-02-05), the Xi'an University of Architecture and Technology Research Initiation Grant Program (No. 1960323102), the Xi'an University of Architecture and Technology Special Program for Cultivation of Frontier Interdisciplinary Fields (No. X20230079), and the Open Fund for the Key Laboratory of Soil and Plant Nutrition of Ningxia (No. ZHS202401).

Author Contributions: Tongtong Wang: Conceptualization, Methodology, Funding acquisition, Project administration, and Writing—review & editing. Zhenhui Pan: Visualization, Data curation, Formal analysis, Investigation, and Writing—original draft. Di Zhang: Visualization and Investigation. Hui Shi: Resources, Supervision, Funding acquisition, and Writing—review & editing. Murat Yilmaz, Amit Kumar, Gaurav Sharma, and Tao Liu: Writing—review & editing. All authors reviewed the results and approved the final version of the manuscript.

Availability of Data and Materials: Not applicable.

Ethics Approval: Not applicable.

Conflicts of Interest: The authors declare no conflicts of interest to report regarding the present study.

References

1. Eikelboom M, Wang Y, Portlock G, Gourain A, Gardner J, Bullen J, et al. Voltammetric determination of inorganic arsenic in mildly acidified (pH 4.7) groundwaters from Mexico and India. *Anal Chim Acta*. 2023;1276:341589. doi:10.1016/j.aca.2023.341589.
2. Mandal BK. Changing concept of arsenic toxicity with development of speciation techniques. In: *Handbook of arsenic toxicology*. Oxford, UK: Academic Press; 2023. p. 193–222.
3. Rahaman MS, Rahman MM, Mise N, Sikder MT, Ichihara G, Uddin MK, et al. Environmental arsenic exposure and its contribution to human diseases, toxicity mechanism and management. *Environ Pollut*. 2021;289:117940. doi:10.1016/j.envpol.2021.117940.
4. World Health Organization. Guidelines for drinking-water quality. 2024 [cited 2024 Dec 31]. Available from: <https://iris.who.int/rest/bitstreams/907844/retrieve>.
5. Inam MA, Khan R, Inam MW, Yeom IT. Kinetic and isothermal sorption of antimony oxyanions onto iron hydroxide during water treatment by coagulation process. *J Water Process Eng*. 2021;41:102050. doi:10.1016/j.jwpe.2021.102050.
6. Bagherifam S, Brown TC, Wijayawardena A, Naidu R. The influence of different antimony (Sb) compounds and ageing on bioavailability and fractionation of antimony in two dissimilar soils. *Environ Pollut*. 2021;270:116270. doi:10.1016/j.envpol.2020.116270.
7. Seal II RR. Economic geology and environmental characteristics of antimony deposits. *Antimony*. 2021;49. doi:10.1515/9783110668711-003.
8. Vidya C.S. N, Shetty R, Vaculik M, Vaculik M. Antimony toxicity in soils and plants, and mechanisms of its alleviation. *Environ Exp Bot*. 2022;202:104996. doi:10.1016/j.envexpbot.2022.104996.
9. Liu L, Supe Tulcan RX, He M, Ouyang W, Zhang Q, Huarez Yarleque CM, et al. Antimony pollution threatens soils and riverine habitats across China: an analysis of antimony concentrations, changes, and risks. *Crit Rev Environ Sci Technol*. 2024;54(10):797–816. doi:10.1080/10643389.2023.2279882.
10. Zhang Z, Lu Y, Li H, Zhang N, Cao J, Qiu B, et al. Simultaneous separation of Sb(III) and Sb(V) by high performance liquid chromatography (HPLC)–inductively coupled plasma-mass spectrometry (ICP-MS) with application to plants, soils, and sediments. *Anal Lett*. 2021;54(6):919–34. doi:10.1080/00032719.2020.1788049.
11. Kumar R, Jing C, Yan L. A critical review on arsenic and antimony adsorption and transformation on mineral facets. *J Environ Sci*. 2024;153:56–75. doi:10.1016/j.jes.2024.01.016.
12. Chen W, Cheng Y, Owens G, Chen Z. Self-immobilized bio-nanomaterials based on hybridized green reduced graphene and *Burkholderia vietnamiensis* C09V for enhanced removal of Sb species from mine wastewater. *Chem Eng J*. 2023;472:145002. doi:10.1016/j.cej.2023.145002.
13. Chen W, Lin Z, Chen Z, Weng X, Owens G, Chen Z. Simultaneous removal of Sb(III) and Sb(V) from mining wastewater by reduced graphene oxide/bimetallic nanoparticles. *Sci Total Environ*. 2022;836:155704. doi:10.1016/j.scitotenv.2022.155704.
14. Li Y, Zhu X, Qi X, Shu B, Zhang X, Li K, et al. Efficient removal of arsenic from copper smelting wastewater in form of scorodite using copper slag. *J Clean Prod*. 2020;270:122428. doi:10.1016/j.jclepro.2020.122428.
15. Qiao W, Wang Y, He P, Yin X, Zhang D, Bai G, et al. Groundwater arsenic and antimony mobility from an antimony mining area: controls of sulfide oxidation, carbonate and silicate weathering, and secondary mineral precipitation. *Water Res*. 2025;273:123086. doi:10.1016/j.watres.2024.123086.
16. Syam Babu D, Nidheesh PV. A review on electrochemical treatment of arsenic from aqueous medium. *Chem Eng Commun*. 2020;208(3):389–410. doi:10.1080/00986445.2020.1715956.
17. Hu Q, Liu Y, Gu X, Zhao Y. Adsorption behavior and mechanism of different arsenic species on mesoporous MnFe_2O_4 magnetic nanoparticles. *Chemosphere*. 2017;181:328–36. doi:10.1016/j.chemosphere.2017.04.049.
18. Yan S, An Q, Xia L, Liu S, Song S, Rangel-Méndez JR. As(V) removal from water using the La(III)-Montmorillonite hydrogel beads. *React Funct Polym*. 2020;147:104456. doi:10.1016/j.reactfunctpolym.2019.104456.
19. Lee SH, Choi H, Kim KW. Removal of As(V) and Sb(V) in water using magnetic nanoparticle-supported layered double hydroxide nanocomposites. *J Geochem Explor*. 2018;184:247–54. doi:10.1016/j.gexplo.2016.11.015.

20. Jeon EK, Ryu S, Park SW, Wang L, Tsang DCW, Baek K. Enhanced adsorption of arsenic onto alum sludge modified by calcination. *J Clean Prod.* 2018;176:54–62. doi:10.1016/j.jclepro.2017.12.153.
21. Jiang H, Tian L, Chen P, Bai Y, Li X, Shu H, et al. Efficient antimony removal by self-assembled core-shell nanocomposite of $\text{Co}_3\text{O}_4/\text{rGO}$ and the analysis of its adsorption mechanism. *Environ Res.* 2020;187:109657. doi:10.1016/j.envres.2020.109657.
22. Xie J, Schofield JRM, Liao L, Peng H, Uppal JS, Zheng Q, et al. Simultaneous removal of arsenic and antimony from mining wastewater. *J Environ Sci.* 2020;9:117–9. doi:10.1016/j.jes.2020.04.003.
23. Yang X, Zhou T, Ren B, Shi Z, Hursthouse A. Synthesis, characterization, and adsorptive properties of $\text{Fe}_3\text{O}_4/\text{GO}$ nanocomposites for antimony removal. *J Anal Methods Chem.* 2017;2017:1–8. doi:10.1155/2017/3012364.
24. Islam A, Teo SH, Ahmed MT, Khandaker S, Ibrahim ML, Vo DVN, et al. Novel micro-structured carbon-based adsorbents for notorious arsenic removal from wastewater. *Chemosphere.* 2021;272:129653. doi:10.1016/j.chemosphere.2021.129653.
25. Yin Z, Cui C, Chen H, Duoni Yu, Qian X, et al. The application of carbon nanotube/graphene-based nanomaterials in wastewater treatment. *Small.* 2019;16(15):1902301. doi:10.1002/sml.201902301.
26. Wang T, Zheng J, Liu H, Peng Q, Zhou H, Zhang X. Adsorption characteristics and mechanisms of Pb^{2+} and Cd^{2+} by a new agricultural waste-Caragana korshinskii biomass derived biochar. *Environ Sci Poll Res.* 2021;28:13800–18.
27. Lehmann J, Joseph S. Biochar for environmental management: science, technology and implementation. 2nd ed. London, UK: Routledge; 2015. doi:10.4324/9780203762264.
28. Fu T, Zhang B, Gao X, Cui S, Guan CY, Zhang Y, et al. Recent progresses, challenges, and opportunities of carbon-based materials applied in heavy metal polluted soil remediation. *Sci Total Environ.* 2023;856:158810. doi:10.1016/j.scitotenv.2022.158810.
29. Aghigh A, Alizadeh V, Wong HY, Islam MDS, Amin N, Zaman M. Recent advances in utilization of graphene for filtration and desalination of water: a review. *Desalination.* 2015;365:389–97. doi:10.1016/j.desal.2015.03.024.
30. Dideikin AT, Vul' AY. Graphene oxide and derivatives: the place in graphene family. *Front Phys.* 2019;6:217. doi:10.3389/fphy.2018.00149.
31. Kovtyukhova NI, Ollivier PJ, Martin BR, Mallouk TE, Chizhik SA, Buzaneva EV, et al. Layer-by-layer assembly of ultrathin composite films from micron-sized graphite oxide sheets and polycations. *Chem Mater.* 1999;11(3):771–8. doi:10.1021/cm981085u.
32. Yahyazadeh A, Nanda S, Dalai AK. Carbon nanotubes: a review of synthesis methods and applications. *Reactions.* 2024;5(3):429–51. doi:10.3390/reactions5030022.
33. Supong A, Sinha UB, Sinha D. Density functional theory calculations of the effect of oxygenated functionals on activated carbon towards cresol adsorption. *Surfaces.* 2022;5(2):280–9. doi:10.3390/surfaces5020020.
34. Cao KLA, Ogi T. Advanced carbon sphere-based hybrid materials produced by innovative aerosol process for high-efficiency rechargeable batteries. *Energy Storage Mater.* 2025;74:103901. doi:10.1016/j.ensm.2024.103901.
35. Cao KLA, Iskandar F, Tanabe E, Ogi T. Recent advances in the fabrication and functionalization of nanostructured carbon spheres for energy storage applications. *Kona Powder Part J.* 2023;40:197–218. doi:10.14356/kona.2023016.
36. Zhou X, Shi L, Moghaddam TB, Chen M, Wu S, Yuan X. Adsorption mechanism of polycyclic aromatic hydrocarbons using wood waste-derived biochar. *J Hazard Mater.* 2022;425:128003. doi:10.1016/j.jhazmat.2021.128003.
37. Wang J, Wang S. Preparation, modification and environmental application of biochar: a review. *J Clean Prod.* 2019;227:1002–22. doi:10.1016/j.jclepro.2019.04.282.
38. Wang T, Zhang D, Shi H, Wang S, Wu B, Jia J, et al. Two birds with one stone: high-quality utilization of COVID-19 waste masks into bio-oil, pyrolytic gas, and eco-friendly biochar with adsorption applications. *C.* 2024;10(3):70. doi:10.3390/c10030070.
39. Amenaghawon AN, Anyalewechi CL, Okieimen CO, Kusuma HS. Biomass pyrolysis technologies for value-added products: a state-of-the-art review. *Environ Dev Sustainability.* 2021;23:14324–78. doi:10.1007/s10668-021-01276-5.
40. Cai N, Zhang H, Nie J, Deng Y, Baeyens J. Biochar from biomass slow pyrolysis. *IOP Conf Ser: Earth Environ Sci.* 2020;586(1):012001. doi:10.1088/1755-1315/586/1/012001.

41. Gürel K, Magalhães D, Kazanç F. The effect of torrefaction, slow, and fast pyrolysis on the single particle combustion of agricultural biomass and lignite coal at high heating rates. *Fuel*. 2022;308:122054. doi:10.1016/j.fuel.2021.122054.
42. Sahoo K, Kumar A, Chakraborty JP. A comparative study on valuable products: bio-oil, biochar, non-condensable gases from pyrolysis of agricultural residues. *J Mater Cycles Waste Manage*. 2021;23:186–204. doi:10.1007/s10163-020-01114-2.
43. Sharma G, Verma Y, Lai CW, Naushad MU, Iqbal J, Kumar A, et al. Biochar and biosorbents derived from biomass for arsenic remediation. *Heliyon*. 2024;10(17):e36288. doi:10.1016/j.heliyon.2024.e36288.
44. Kim KH, Kim TS, Lee SM, Choi D, Yeo H, Choi IG, et al. Comparison of physicochemical features of biooils and biochars produced from various woody biomasses by fast pyrolysis. *Renew Energy*. 2013;50:188–95. doi:10.1016/j.renene.2012.06.030.
45. Dai Y, Zhang N, Xing C, Cui Q, Sun Q. The adsorption, regeneration and engineering applications of biochar for removal organic pollutants: a review. *Chemosphere*. 2019;223:12–27. doi:10.1016/j.chemosphere.2019.01.161.
46. Zheng Y, Shao Y, Li B. Analysis of biomass gasification technology principles and applications. *Dist Heat*. 2010;3:39–42. doi:10.16641/j.cnki.cn11-3241/tk.2010.03.018.
47. Sevilla M, Fuertes AB. The production of carbon materials by hydrothermal carbonization of cellulose. *Carbon*. 2009;47(9):2281–9. doi:10.1016/j.carbon.2009.04.026.
48. Liu Z, Quek A, Kent Hoekman S, Balasubramanian R. Production of solid biochar fuel from waste biomass by hydrothermal carbonization. *Fuel*. 2013;103:943–9. doi:10.1016/j.fuel.2012.07.069.
49. Novoselov KS, Geim AK, Morozov SV, Jiang D, Zhang Y, Dubonos SV, et al. Electric field effect in atomically thin carbon films. *Science*. 2004;306(5696):666–9. doi:10.1126/science.1102896.
50. Tabish TA, Memon FA, Gomez DE, Horsell DW, Zhang S. A facile synthesis of porous graphene for efficient water and wastewater treatment. *Sci Rep*. 2018;8(1):1817. doi:10.1038/s41598-018-19978-8.
51. Das S, Singh S, Singh V, Joung D, Dowding JM, Reid D, et al. Oxygenated functional group density on graphene oxide: its effect on cell toxicity. *Part Part Syst Charact*. 2013;30(2):148–57. doi:10.1002/ppsc.201200066.
52. Huang J, Zhao X, Huang H, Wang Z, Li J, Li Z, et al. Scalable production of few layered graphene by soft ball-microsphere rolling transfer. *Carbon*. 2019;154:402–9. doi:10.1016/j.carbon.2019.08.026.
53. Obraztsov AN. Making graphene on a large scale. *Nat Nanotechnol*. 2009;4(4):212–3. doi:10.1038/nnano.2009.67.
54. Ding G, Zhu Y, Wang S, Gong Q, Sun L, Wu T, et al. Chemical vapor deposition of graphene on liquid metal catalysts. *Carbon*. 2013;53:321–6. doi:10.1016/j.carbon.2012.11.018.
55. Chua CK, Pumera M. Chemical reduction of graphene oxide: a synthetic chemistry viewpoint. *Chem Soc Rev*. 2014;43(1):291–312. doi:10.1039/C3CS60303B.
56. Iijima S. Helical microtubules of graphitic carbon. *Nature*. 1991;354(6348):56–8. doi:10.1038/354056a0.
57. Arunkumar T, Karthikeyan R, Ram Subramani R, Viswanathan K, Anish M. Synthesis and characterisation of multi-walled carbon nanotubes (MWCNTs). *Int J Ambient Energy*. 2018;41(4):452–6. doi:10.1080/01430750.2018.1472657.
58. Rahman G, Najaf Z, Mehmood A, Bilal S, Shah A, Mian S, et al. An overview of the recent progress in the synthesis and applications of carbon nanotubes. *C*. 2019;5(1):3. doi:10.3390/c5010003.
59. Cadek M, Murphy R, McCarthy B, Drury A, Lahr B, Barklie RC, et al. Optimisation of the arc-discharge production of multi-walled carbon nanotubes. *Carbon*. 2002;40(6):923–8. doi:10.1016/S0008-6223(01)00221-4.
60. Sarangdevot K, Sonigara BS. The wondrous world of carbon nanotubes: structure, synthesis, properties and applications. *J Chem Pharm Res*. 2015;7:916–33.
61. Thess A, Lee R, Nikolaev P, Dai H, Petit P, Robert J, et al. Crystalline ropes of metallic carbon nanotubes. *Science*. 1996;273(5274):483–7. doi:10.1126/science.273.5274.483.
62. Daenen M, De Fouw RD, Hamers B, Janssen PGA, Schouteden K, Veld MAJ. The wondrous world of carbon nanotubes. A review of current carbon nanotube technologies. *Eindh Univ Technol*. 2003;1:96.
63. Cassell AM, Raymakers JA, Kong J, Dai H. Large scale CVD synthesis of single-walled carbon nanotubes. *J Phys Chem B*. 1999;103(31):6484–92. doi:10.1021/jp990957s.
64. Heidarinejad Z, Dehghani MH, Heidari M, Javedan G, Ali I, Sillanpää M. Methods for preparation and activation of activated carbon: a review. *Environ Chem Lett*. 2020;18(2):393–415. doi:10.1007/s10311-019-00955-0.

65. Bouchelta C, Medjram MS, Bertrand O, Bellat JP. Preparation and characterization of activated carbon from date stones by physical activation with steam. *J Anal Appl Pyrolysis*. 2008;82(1):70–7. doi:10.1016/j.jaap.2007.12.009.
66. Zhou J, Luo A, Zhao Y. Preparation and characterisation of activated carbon from waste tea by physical activation using steam. *J Air Waste Manage Assoc*. 2018;68(12):1269–77. doi:10.1080/10962247.2018.1460282.
67. Yahya MA, Al-Qodah Z, Ngah CWZ. Agricultural bio-waste materials as potential sustainable precursors used for activated carbon production: a review. *Renew Sustain Energy Rev*. 2015;46:218–35. doi:10.1016/j.rser.2015.02.051.
68. Jiang JC, Sun K. Review on preparation technology of activated carbon and its application. *Chem Ind For Prod*. 2017;37(1):1–13. doi:10.3969/j.issn.0253-2417.2017.01.001.
69. Samsuri AW, Sadegh-Zadeh F, Seh-Bardan BJ. Characterization of biochars produced from oil palm and rice husks and their adsorption capacities for heavy metals. *Int J Environ Sci Technol*. 2013;11(4):967–76. doi:10.1007/s13762-013-0291-3.
70. Hayashi JI, Kazezaya A, Muroyama K, Watkinson AP. Preparation of activated carbon from lignin by chemical activation. *Carbon*. 2000;38(13):1873–8. doi:10.1016/S0008-6223(00)00027-0.
71. Lagergren S. About the theory of so-called adsorption of soluble substances. *Kungliga Svenska Vetenskap-sakademiens Handlingar Band*. 1898;24:1–39.
72. Ho YS, Wang CC. Pseudo-isotherms for the sorption of cadmium ion onto tree fern. *Process Biochem*. 2004;39(6):761–5. doi:10.1016/S0032-9592(03)00184-5.
73. Ho YS. Review of second-order models for adsorption systems. *J Hazard Mater*. 2006;136(3):681–9. doi:10.1016/j.jhazmat.2005.12.043.
74. Zhang D, Wang T, Zhi J, Zheng Q, Chen Q, Zhang C, et al. Utilization of Jujube biomass to prepare biochar by pyrolysis and activation: characterization, adsorption characteristics, and mechanisms for nitrogen. *Materials*. 2020;13(24):5594. doi:10.3390/ma13245594.
75. Navarathna CM, Karunanayake AG, Gunatilake SR, Pittman CU, Perez F, Mohan D, et al. Removal of Arsenic(III) from water using magnetite precipitated onto Douglas fir biochar. *J Environ Manage*. 2019;250:109429. doi:10.1016/j.jenvman.2019.109429.
76. Ye Y, Yin D, Wang B, Zhang Q. Synthesis of three-dimensional Fe₃O₄/graphene aerogels for the removal of arsenic ions from water. *Yu WW, ed. J Nanomater*. 2015;2015(1):864864. doi:10.1155/2015/864864.
77. Ma MD, Wu H, Deng ZY, Zhao X. Arsenic removal from water by nanometer iron oxide coated single-wall carbon nanotubes. *J Mol Liq*. 2018;259:369–75. doi:10.1016/j.molliq.2018.03.052.
78. Sawana R, Somasundar Y, Iyer VS, Baruwati B. Ceria modified activated carbon: an efficient arsenic removal adsorbent for drinking water purification. *Appl Water Sci*. 2017;7(3):1223–30. doi:10.1007/s13201-016-0398-z.
79. Wang TT, Ma JB, Qu D, Zhang XY, Zheng JY, Zhang XC. Characteristics and mechanism of copper adsorption from aqueous solutions on biochar produced from sawdust and apple branch. *Environ Sci*. 2017;38(5):2161–71. doi:10.13227/j.hjlx.201610124.
80. Deng S, Ren B, Hou B, Deng X, Deng R, Zhu G, et al. Adsorption of Sb(III) and Pb(II) in wastewater by magnetic γ -Fe₂O₃-loaded sludge biochar: performance and mechanisms. *Chemosphere*. 2024;349:140914. doi:10.1016/j.chemosphere.2023.140914.
81. Jia X, Zhou J, Liu J, Liu P, Yu L, Wen B, et al. The antimony sorption and transport mechanisms in removal experiment by Mn-coated biochar. *Sci Total Environ*. 2020;724:138158. doi:10.1016/j.scitotenv.2020.138158.
82. Salam MA, Mohamed RM. Removal of antimony(III) by multi-walled carbon nanotubes from model solution and environmental samples. *Chem Eng Res Des*. 2013;91(7):1352–60. doi:10.1016/j.cherd.2013.02.007.
83. Liu Y, Meng L, Han K, Sun S. Synthesis of nano-zirconium-iron oxide supported by activated carbon composite for the removal of Sb(V) in aqueous solution. *RSC Adv*. 2021;11(49):31131–41. doi:10.1039/D1RA06117H.
84. Langmuir I. The constitution and fundamental properties of solids and liquids. Part I. Solids. *J Am Chem Soc*. 1916;38(11):2221–95. doi:10.1021/ja02268a002.
85. Freundlich H. Über die Adsorption in Lösungen. *Z Für Phys Chem*. 1907;57U(1):385–470. doi:10.1515/zpch-1907-5723.

86. Mukherjee S, Thakur AK, Goswami R, Mazumder P, Taki K, Vithanage M, et al. Efficacy of agricultural waste derived biochar for arsenic removal: tackling water quality in the Indo-Gangetic plain. *J Environ Manage.* 2021;281:111814. doi:10.1016/j.jenvman.2020.111814.
87. Kumar S, Nair RR, Pillai PB, Gupta SN, Iyengar MAR, Sood AK. Graphene Oxide–MnFe₂O₄ Magnetic Na-nohybrids for Efficient Removal of Lead and Arsenic from Water. *ACS Appl Mater Interfaces.* 2014;6(20):17426–17436. doi:10.1021/am504826q.
88. Gallios G, Tolkou A, Katsoyiannis I, Stefusova K, Vaclavikova M, Deliyanni E. Adsorption of arsenate by nano scaled activated carbon modified by iron and manganese oxides. *Sustainability.* 2017;9(10):1684. doi:10.3390/su9101684.
89. Dong S, Dou X, Mohan D, Pittman CU, Luo J. Synthesis of graphene oxide/schwertmannite nanocomposites and their application in Sb(V) adsorption from water. *Chem Eng J.* 2015;270:205–14. doi:10.1016/j.cej.2015.01.071.
90. Egbosiuba TC, Abdulkareem AS, Kovo AS, Afolabi EA, Tijani JO, Roos WD. Enhanced adsorption of As(V) and Mn(VII) from industrial wastewater using multi-walled carbon nanotubes and carboxylated multi-walled carbon nanotubes. *Chemosphere.* 2020;254:126780. doi:10.1016/j.chemosphere.2020.126780.
91. Saleh TA, Sari A, Tuzen M. Effective adsorption of antimony(III) from aqueous solutions by polyamide-graphene composite as a novel adsorbent. *Chem Eng J.* 2017;307:230–8. doi:10.1016/j.cej.2016.08.070.
92. Veličković Z, Bajić Z, Ristić M, Djokic V, Marinkovic A, Uskokovic P, et al. Modification of multi-wall carbon nanotubes for the removal of cadmium, lead and arsenic from wastewater. *Dig J Nanomater Biostruct.* 2013;8:501–11.
93. Leng Y, Guo W, Su S, Yi C, Xing L. Removal of antimony(III) from aqueous solution by graphene as an adsorbent. *Chem Eng J.* 2012;211–212:406–11. doi:10.1016/j.cej.2012.09.078.
94. Nidheesh PV, Divyapriya G, Cerkez EB, Gopinath A, Banerji T, Strongin DR. Oxidative sorption of arsenite from water by iron: a mechanistic perspective. *Environ Sci Water Res Technol.* 2022;8(11):2466–90. doi:10.1039/D2EW00522K.
95. Wang J, Sun M, Wang L, Xiong X, Yuan W, Liu Y, et al. High-efficiency removal of arsenic(III) from wastewater using combined copper ferrite@biochar and persulfate. *Chemosphere.* 2023;336:139089. doi:10.1016/j.chemosphere.2023.139089.
96. Kumar ASK, Jiang SJ. Chitosan-functionalized graphene oxide: a novel adsorbent an efficient adsorption of arsenic from aqueous solution. *J Environ Chem Eng.* 2016;4(2):1698–713. doi:10.1016/j.jece.2016.02.035.
97. Kang M, Kawasaki M, Tamada S, Kamei T, Magara Y. Effect of pH on the removal of arsenic and antimony using reverse osmosis membranes. *Desalination.* 2000;131(1–3):293–8. doi:10.1016/S0011-9164(00)90027-4.
98. Yu TC, Wang XH, Li C. Removal of antimony by FeCl₃-modified granular-activated carbon in aqueous solution. *J Environ Eng.* 2014;140(9):A4014001. doi:10.1061/(ASCE)EE.1943-7870.0000736.
99. Deng J, Li X, Wei X, Liu Y, Liang J, Shao Y, et al. Different adsorption behaviors and mechanisms of a novel amino-functionalized hydrothermal biochar for hexavalent chromium and pentavalent antimony. *Bioresour Technol.* 2020;310:123438. doi:10.1016/j.biortech.2020.123438.
100. Chen G, Liu X, Su C. Distinct effects of humic acid on transport and retention of TiO₂ rutile nanoparticles in saturated sand columns. *Environ Sci Technol.* 2012;46(13):7142–50. doi:10.1021/es204010g.
101. Li R, Li Q, Gao S, Shang JK. Exceptional arsenic adsorption performance of hydrous cerium oxide nanoparticles: part A. Adsorption capacity and mechanism. *Chem Eng J.* 2012;185–186:127–35. doi:10.1016/j.cej.2012.01.061.
102. Mishra S, Dwivedi J, Kumar A, Sankararamakrishnan N. Removal of antimonite (Sb(III)) and antimonate (Sb(V)) using zerovalent iron decorated functionalized carbon nanotubes. *RSC Adv.* 2016;6(98):95865–78. doi:10.1039/C6RA18965B.
103. Yin HQ, Guo C, Hu J, Gao XP, Li MY. Adsorption of arsenic ions from water by biomass derived materials: a review. *Chem Ind Eng.* 2022;39(4):71–82. doi:10.13353/j.issn.1004.9533.20216003.
104. Liu XY, Liu JJ, Ke Y, Yan X. Progress in the study of the morphology and transformation pattern of antimony in water bodies. *Chin J Nonferrous Met.* 2021;31(5):1330–46. doi:10.11817/j.ysxb.1004.0609.2021-36569.
105. Herath I, Vithanage M, Bundschuh J. Antimony as a global dilemma: geochemistry, mobility, fate and transport. *Environ Pollut.* 2017;223:545–59. doi:10.1016/j.envpol.2017.01.057.

106. Yang X, Wan Y, Zheng Y, He F, Yu Z, Huang J, et al. Surface functional groups of carbon-based adsorbents and their roles in the removal of heavy metals from aqueous solutions: a critical review. *Chem Eng J*. 2019;366:608–21. doi:10.1016/j.cej.2019.02.119.
107. Nieto-Delgado C, Rangel-Mendez JR. Anchorage of iron hydro(oxide) nanoparticles onto activated carbon to remove As(V) from water. *Water Res*. 2012;46(9):2973–82. doi:10.1016/j.watres.2012.03.026.
108. Dong L, Hou L, Wang Z, Gu P, Chen G, Jiang R. A new function of spent activated carbon in BAC process: removing heavy metals by ion exchange mechanism. *J Hazard Mater*. 2018;359:76–84. doi:10.1016/j.jhazmat.2018.07.030.
109. Luo M, Lin H, He Y, Li B, Dong Y, Wang L. Efficient simultaneous removal of cadmium and arsenic in aqueous solution by titanium-modified ultrasonic biochar. *Bioresour Technol*. 2019;284:333–9. doi:10.1016/j.biortech.2019.03.108.
110. Qiu B, Shao Q, Shi J, Yang C, Chu H. Application of biochar for the adsorption of organic pollutants from wastewater: modification strategies, mechanisms and challenges. *Sep Purif Technol*. 2022;300:121925. doi:10.1016/j.seppur.2022.121925.
111. Sattar MS, Shakoor MB, Ali S, Rizwan M, Niazi NK, Jilani A. Comparative efficiency of peanut shell and peanut shell biochar for removal of arsenic from water. *Environ Sci Pollut Res*. 2019;26(18):18624–35. doi:10.1007/s11356-019-05185-z.
112. Lingamdinne LP, Choi JS, Choi YL, Chang YY, Yang JK, Karri RR, et al. Process modeling and optimization of an iron oxide immobilized graphene oxide gadolinium nanocomposite for arsenic adsorption. *J Mol Liq*. 2020;299:112261. doi:10.1016/j.molliq.2019.112261.
113. Peng W, Li H, Liu Y, Song S. A review on heavy metal ions adsorption from water by graphene oxide and its composites. *J Mol Liq*. 2017;230:496–504. doi:10.1016/j.molliq.2017.01.064.
114. Shaikh WA, Alam MDA, Alam MDO, Chakraborty S, Owens G, Bhattacharya T, et al. Enhanced aqueous phase arsenic removal by a biochar based iron nanocomposite. *Environ Technol Innov*. 2020;19:100936. doi:10.1016/j.eti.2020.100936.
115. Cheng Z, Lyu H, Shen B, Tian J, Sun Y, Wu C. Removal of antimonite (Sb(III)) from aqueous solution using a magnetic iron-modified carbon nanotubes (CNTs) composite: experimental observations and governing mechanisms. *Chemosphere*. 2022;288:132581. doi:10.1016/j.chemosphere.2021.132581.
116. Li L, Liao L, Wang B, Li W, Liu T, Wu P, et al. Effective Sb(V) removal from aqueous solution using phosphogypsum-modified biochar. *Environ Pollut*. 2022;301:119032. doi:10.1016/j.envpol.2022.119032.
117. Bai Y, Wu F, Gong Y. Oxidation and adsorption of antimony(III) from surface water using novel Al₂O₃-supported Fe-Mn binary oxide nanoparticles: Effectiveness, dynamic quantitative mechanisms, and life cycle analysis. *Environ Sci Nano*. 2020;7(10):3047–61. doi:10.1039/D0EN00609B.
118. Liu S, Feng H, Tang L, Dong H, Wang J, Yu J, et al. Removal of Sb(III) by sulfidated nanoscale zerovalent iron: the mechanism and impact of environmental conditions. *Sci Total Environ*. 2020;736:139629. doi:10.1016/j.scitotenv.2020.139629.
119. Peng L, Wang N, Xiao T, Wang J, Quan H, Fu C, et al. A critical review on adsorptive removal of antimony from waters: adsorbent species, interface behavior and interaction mechanism. *Chemosphere*. 2023;327:138529. doi:10.1016/j.chemosphere.2023.138529.
120. Zhang F, Wang X, Xionghui J, Ma L. Efficient arsenate removal by magnetite-modified water hyacinth biochar. *Environ Pollut*. 2016;216:575–83. doi:10.1016/j.envpol.2016.06.013.
121. Yu F, Sun S, Ma J, Han S. Enhanced removal performance of arsenate and arsenite by magnetic graphene oxide with high iron oxide loading. *Phys Chem Chem Phys*. 2015;17(6):4388–97. doi:10.1039/C4CP04835K.
122. Shahrin S, Lau WJ, Goh PS, Jaafar J, Ismail AF. Adsorptive removal of As(V) ions from water using graphene oxide-manganese ferrite and titania nanotube-manganese ferrite hybrid nanomaterials. *Chem Eng Technol*. 2018;41(11):2250–8. doi:10.1002/ceat.201800322.
123. Chen B, Zhu Z, Ma J, Yang M, Hong J, Hu X, et al. One-pot, solid-phase synthesis of magnetic multiwalled carbon nanotube/iron oxide composites and their application in arsenic removal. *J Coll Interface Sci*. 2014;434:9–17. doi:10.1016/j.jcis.2014.07.046.

124. Addo Ntim S, Mitra S. Adsorption of arsenic on multiwall carbon nanotube-zirconia nanohybrid for potential drinking water purification. *J Coll Interface Sci.* 2012;375(1):154–9. doi:10.1016/j.jcis.2012.01.063.
125. Asadullah M, Jahan I, Ahmed MB, Adawiyah P, Malek NH, Rahman MS. Preparation of microporous activated carbon and its modification for arsenic removal from water. *J Ind Eng Chem.* 2014;20(3):887–96. doi:10.1016/j.jiec.2013.06.019.
126. Chen W, Parette R, Zou J, Cannon FS, Dempsey BA. Arsenic removal by iron-modified activated carbon. *Water Res.* 2007;41(9):1851–8. doi:10.1016/j.watres.2007.01.052.
127. Wang L, Wang J, Wang Z, He C, Lyu W, Yan W, et al. Enhanced antimonate (Sb(V)) removal from aqueous solution by La-doped magnetic biochars. *Chem Eng J.* 2018;354:623–32. doi:10.1016/j.cej.2018.08.074.
128. Yao B, Li Y, Zeng W, Yang G, Zeng J, Nie J, et al. Synergistic adsorption and oxidation of trivalent antimony from groundwater using biochar supported magnesium ferrite: performances and mechanisms. *Environ Pollut.* 2023;323:121318. doi:10.1016/j.envpol.2023.121318.
129. Park SJ, Lee YJ, Kang JK, Lee JC, Lee CG. Application of Fe-impregnated biochar from cattle manure for removing pentavalent antimony from aqueous solution. *Appl Sci.* 2021;11(19):9257. doi:10.3390/app11199257.
130. Cui X, Ni Q, Lin Q, Khan KY, Li T, Khan MB, et al. Simultaneous sorption and catalytic oxidation of trivalent antimony by *Canna indica* derived biochars. *Environ Pollut.* 2017;229:394–402. doi:10.1016/j.envpol.2017.06.005.
131. Liu X, Zhou J, Zhou W, Feng Y, Finfrook YZ, Liu Y, et al. Efficiency and mechanisms of Sb(III/V) removal by Fe-modified biochars using X-ray absorption spectroscopy. *J Environ Chem Eng.* 2021;9(6):106741. doi:10.1016/j.jece.2021.106741.
132. Ji J, Xu S, Ma Z, Mou Y. Optimisation of preparation conditions and removal mechanism for trivalent antimony by biochar-supported nano zero-valent iron. *Environ Technol Innov.* 2022;26:102240. doi:10.1016/j.eti.2021.102240.
133. Lai L, Liu X, Ren W, Zhou Z, Zhao X, Zeng X, et al. Efficient removal of Sb(III) from water using β -FeOOH-modified biochar: synthesis, performance and mechanism. *Chemosphere.* 2023;311:137057. doi:10.1016/j.chemosphere.2022.137057.
134. Chi Z, Ju S, Liu X, Sun F, Zhu Y. Graphene oxide supported sulfidated nano zero-valent iron (S-nZVI@GO) for antimony removal: the role of active oxygen species and reaction mechanism. *Chemosphere.* 2022;308:136253. doi:10.1016/j.chemosphere.2022.136253.
135. Sharma PK, Kumar R, Singh RK, Sharma P, Ghosh A. Review on arsenic removal using biochar-based materials. *Groundw Sustain Dev.* 2022;17:100740. doi:10.1016/j.gsd.2022.100740.
136. Zhang X, Xie N, Guo Y, Niu D, Sun H-B, Yang Y. Insights into adsorptive removal of antimony contaminants: functional materials, evaluation and prospective. *J Hazard Mater.* 2021;418:126345.
137. Wang T, Li G, Yang K, Zhang X, Wang K, Cai J, et al. Enhanced ammonium removal on biochar from a new forestry waste by ultrasonic activation: characteristics, mechanisms and evaluation. *Sci Total Environ.* 2021;778:146295. doi:10.1016/j.scitotenv.2021.146295.
138. Zou JP, Liu HL, Luo J, Xing QJ, Du HM, Jiang XH, et al. Three-dimensional reduced graphene oxide coupled with Mn_3O_4 for highly efficient removal of Sb(III) and Sb(V) from water. *ACS Appl Mater Interfaces.* 2016;8(28):18140–9. doi:10.1021/acsami.6b05895.
139. Pan X, Wu S, Chen J, Zhou X, Chen X, Xin Z, et al. Toward efficient biofuel production: a review of online upgrading methods for biomass pyrolysis. *Energy Fuels.* 2024;38(20):19414–41.
140. Gabris MA, Rezanian S, Rafieizonooz M, Khankhaje E, Devanesan S, AlSalhi MS, et al. Chitosan magnetic graphene grafted polyaniline doped with cobalt oxide for removal of Arsenic(V) from water. *Environ Res.* 2022;207:112209.
141. Jaiswal VK, Gupta AD, Kushwaha R, Kumar R, Singh K, Singh H, et al. Arsenic removal from water using an acid-modified biochar. *J Mol Struct.* 2025;1324:140904. doi:10.1016/j.molstruc.2024.140904.